

Martini 3 Coarse-Grained Models for Carbon Nanomaterials

Roshan Shrestha, Riccardo Alessandri, Martin Vögele, Cecile Hilpert, Paulo C. T. Souza, Siewert J. Marrink, and Luca Monticelli*



Cite This: <https://doi.org/10.1021/acs.jctc.5c00923>



Read Online

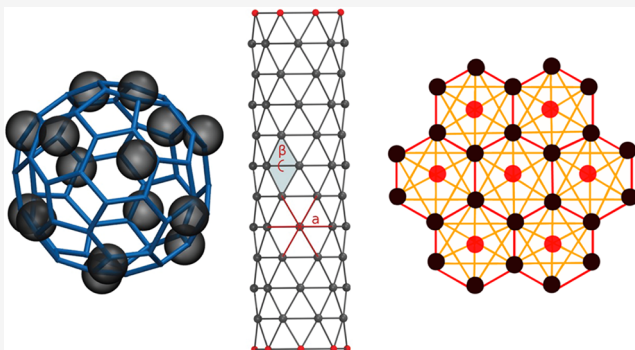
ACCESS |

Metrics & More

Article Recommendations

Supporting Information

ABSTRACT: The Martini model is a coarse-grained force field allowing simulations of biomolecular systems as well as a range of materials including different types of nanomaterials of technological interest. Recently, a new version of the force field (version 3) has been released that includes new parameters for lipids, proteins, carbohydrates, and a number of small molecules, but not yet carbon nanomaterials. Here, we present new Martini models for three major types of carbon nanomaterials: fullerene, carbon nanotubes, and graphene. The new models were parametrized within the Martini 3 framework, and reproduce semiquantitatively a range of properties for each material. In particular, the model of fullerene yields excellent solid-state properties and good properties in solution, including correct trends in partitioning between different solvents and realistic translocation across lipid membranes. The models of carbon nanotubes reproduce the atomistic behavior of nanotube porins spanning lipid bilayers. The model of graphene reproduces structural and elastic properties, as well as trends in experimental adsorption enthalpies of organic molecules. All new models can be used in large-scale simulations to study the interaction with the wide variety of molecules already available in the Martini 3 force field, including biomolecular and synthetic systems.



INTRODUCTION

The emergence of nanotechnology has revolutionized different industrial sectors.¹ This revolution is driven by the capability to synthesize and use nanosized materials, with sizes that are less than 100 nm in dimension.² Among different nanomaterials, carbon nanomaterials (CNMs) have attracted considerable attention because of their unique electrical, optical, thermal, mechanical, and chemical properties, which offer a wide range of applications in several industrial sectors, such as optoelectronics, sensors, and medicine. For instance, CNM-enabled technologies are being developed to enhance energy storage systems, which play a critical role in renewable energy integration and reducing greenhouse gas emissions,^{3–5} both of which are paramount to achieving carbon neutrality in the long run. With the rise in CNMs production, it has become necessary to adopt safe-and-sustainable-by-design principles from the early stages of development of new products.⁶ To this end, molecular-level modeling has increasingly been used to predict the properties of CNMs and CNM-based multi-component materials. Simulations of CNMs in complex media, including environmental and biological media, have been used to predict interactions at atomic resolution, which are difficult to observe with experimental techniques but very relevant in the context of biodistribution and accumulation and potentially useful in the exploration of some mechanisms of toxicity. In particular, molecular dynamics (MD) simulations are a

powerful tool in understanding both materials properties and bionano interactions.^{7–16} MD simulations at the atomistic level provide insight into the properties of CNMs at length scales up to a few tens of nanometers and time scales up to microseconds, but larger length and time scales generally require the use of coarse-grained (CG) force fields or continuum models. Among CG force fields, the Martini model¹⁷ has often been used for the study of bionano interactions,^{7,8,12,18,19} as well as in materials science.²⁰ In Martini, each CG particle type is parametrized to reproduce the partitioning of the corresponding chemical moiety between different solvents. However, the lack of experimental data on partitioning is a major difficulty in the development of Martini models for CNMs.¹⁸ In the case of C₆₀ fullerene, solubilities in different solvents are available, and these can be used to estimate the partitioning between solvents and, therefore, to develop a coarse-grained model compatible with the Martini framework. However, in version 2 of the force field, no available particle type could reproduce fullerene partitioning in

Received: June 6, 2025

Revised: August 8, 2025

Accepted: August 22, 2025

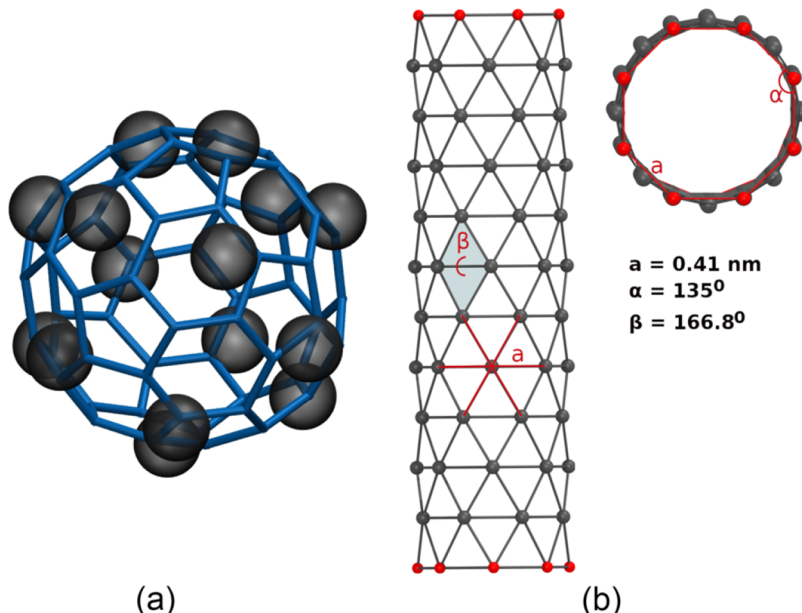


Figure 1. (a) Representation of the atomistic molecular structure of fullerene (blue) and its CG representation (black). (b) Structure of a Martini 3 model of a carbon nanotube, with nonpolar SCS particle types (in gray) in all positions except for the polar capping groups (in red). Angles (a, b) and bonds (a) are indicated.

a satisfactory way, and we resorted to the use of an optimized particle type,^{15,21} reproducing partitioning, solid-state properties (available from experiments), and interactions with lipid membranes (as derived from atomistic simulations). Martini models for carbon nanotubes (CNTs)^{13,22,14} were based on the parameters developed for fullerene^{15,21} and were used in studies on membrane fusion¹² and as probes for membrane diffusion.^{23,24} Martini models of graphite, instead, also used a customized particle, optimized based on experimental data,²⁵ such as enthalpies of adsorption, wetting enthalpies of pure liquids, and enthalpies of displacement of long-chain organic molecules from different solvents.²⁵ In the case of graphite, not only the specific Lennard-Jones (LJ) parameters needed to be optimized, but also the mapping (with a 2-to-1 ratio of carbon atoms to CG particles²⁵). A subsequent model of graphene and graphene oxide adopted the parameters developed for graphite.²⁶ Furthermore, Williams and Lisal developed a model of graphene and graphene oxide compatible with the polarizable Martini water model by reproducing the all-atom (AA) graphene/graphene oxide-water radial distribution function (RDF) and sheet–sheet aggregation free energies.²⁷ These models were suitable for studying the behavior of lipids on these CNMs, and their interaction with water.^{14,19,27–29} Overall, Martini 2 models of different carbon nanomaterials were developed with very different strategies, which was necessary mostly due to the small number of particles available in the force field and the imperfect balance of interactions among particles of different sizes.

Version 3 of the Martini force field features an improved balance of interactions among particles of different sizes, along with many new particle types, and offers numerous possibilities to explore both biomolecular systems and synthetic materials—broader in variety compared to the previous versions of the force field.³⁰ Unfortunately, due to recalibration of most interactions, previously developed models for CNMs are not compatible with version 3 of the force field.

Here, we present new Martini models for three types of carbon nanomaterials: C₆₀ fullerene, carbon nanotubes, and graphene, all compatible with version 3 of the force field. Models for fullerene and CNTs represent updates of previous Martini 2 models as they use the same mapping and the same target properties; the model for graphene, instead, is new in terms of mapping and the choice of target properties. The rest of the paper is structured as follows: first, we present the parametrization strategy for each model, and then we validate our models by comparing their properties with results from AA simulations and/or experiments. Finally, we discuss the applicability and limitations of these models.

■ DEVELOPMENT OF THE FULLERENE MODEL: MAPPING

In Martini, particles of three different sizes exist, generally corresponding to different mappings; “regular” size particles are used for 4:1 mapping (meaning that 4 nonhydrogen atoms are mapped onto 1 coarse-grained particle), “small” size for 3:1 mapping, and “tiny” size for 2:1 mapping. Branching is considered to reduce the size of CG particles; therefore, “small” CG particles are used in the case of 4:1 mapping when the atomistic structure is branched.³⁰ In the case of C₆₀ fullerene, different choices are possible for mapping, leading to CG models with different numbers of particles. Here we followed the choice made in version 2 of the model,²¹ using small CG particles with a 4:1 mapping (due to the branched structure), which leads to models with 15 particles. Notice that some degree of fuzziness remains in the mapping, which allows for some flexibility in the choice of the exact number of particles to be used; indeed, 16 particles were used in the Martini 2 model, as this simplified the optimization of several target properties at the same time.

In the new Martini 3 model of C₆₀, the initial structure was generated by placing 15 particles on a spherical surface with a diameter of 0.73 nm (corresponding to the real size of C₆₀ fullerene) and maximizing the interparticle distances using a

Monte Carlo method²¹ (Figure 1a). The program to generate this structure is the same used for Martini 2 models and is available online at <https://github.com/MoMS-MMSB/Martini3-Fullerene>. The initial choice of particle chemical type was SC5, by analogy with the TC5 type used in Martini 3 to represent benzene. In Martini 3, the C5 chemical type is also generally used for conjugated carbon-based molecules. The CG particles were connected with an elastic network of bonds, with a force constant of 1250 kJ/mol nm², adapted from the Martini 2 model.²¹

■ DEVELOPMENT OF THE FULLERENE MODEL: BONDED INTERACTIONS

Enthalpy of sublimation (ΔH_{sub}) and the lattice constant are important solid-state properties of a crystal. The enthalpy of sublimation is related to the cohesive forces in the solid, while the lattice constant defines the size of the unit cell and the packing of particles in the crystal. In the parametrization of Martini models, solid-state properties are generally not the main target, but they are quite important in the case of fullerene as we wish to reproduce in a reasonable way fullerene aggregation in solution, as in the previous version^{15,21} of the model; packing of fullerene clusters formed in solution strongly depends on packing in the solid state.

Here, we tested fullerene models with different sizes and different numbers of particles (between 15 and 21), and then optimized the bonded parameters (related to the radius of the molecule) to reproduce the lattice constant and enthalpy of sublimation. As the latter also depends on nonbonded interactions, the optimization required an iterative procedure, with optimization of both bonded and nonbonded interactions.

The only models that could reproduce solid-state properties reasonably well were F15 and F16, consisting of 15 and 16 particles, respectively (see Table S2). After optimization of nonbonded interactions (see the following section), the F15 model was selected as the model of choice; parameters for the optimized model are reported in Table 1. The lattice constant

Table 1. Enthalpy of Sublimation and Lattice Constant for a Face-Centered Crystal of F15, Using the SC5r Particle Type^a

	radius (nm)	ΔH_{sub} (kJ/mol)	lattice constant (nm)
F15 model (Martini 3)	0.365	158 ± 1	1.42 ± 0.01
all-atom (Girifalco ²⁸)	0.35	178.4 ± 0.3	1.417 ± 0.0004
experiment	0.35	180 ± 3	1.417

^aThe “radius” refers to the radius of the sphere whose surface contains all of the CG particles.

matches well both the experimental³¹ and all-atom (Girifalco)^{32,33} values. The computed value for ΔH_{sub} is underestimated by about 12%, but it is closer to the experimental value³⁴ compared to the previous Martini 2 model²¹ (210–220 kJ/mol). It should be noted that Martini 3 models generally underestimate both enthalpies of sublimation and enthalpies of vaporization (ΔH_{vap}).^{30,35} We therefore consider the current model satisfactory in this respect.

■ DEVELOPMENT OF THE FULLERENE MODEL: NONBONDED INTERACTIONS

Partitioning between different solvents is one of the main targets for the parametrization of nonbonded interactions in

the Martini force field. We calculated free energies of transfer for our fullerene model between 7 pairs of solvents: benzene, octane, cyclohexane, acetone, 1-butanol, ethanol, and water. We first used our initial guess for the particle type, i.e., SC5, and then other similar particle types (see Supporting Information S2). Fullerene models with different numbers of particles were also tested; overall, we tested 13 different fullerene models, including 7 with different numbers of particles (between 15 and 21 particles) and 6 with different particle types. This is because, as mentioned above, solid-state properties were not the main target in this parametrization, and we intended to strike a balance between different properties, with an emphasis on fullerene properties, in solution.

For each of the tested fullerene models, we calculated 7 free energies of solvation, yielding a total number of 91 free energy calculations. In Supporting Information, we report the results for selected cases (Tables S3–S8). To compare different models, we calculated the mean unsigned error (i.e., the absolute difference between calculated and experimental data) in the free energies of transfer, and used it as a quantitative criterion to select the best model. Due to the high uncertainty in the experimental measures in water,³⁶ free energies of transfer into water were not used as a target. Among the different models tested, the F15 model (i.e., the model with 15 particles) and the SC5 particle type performed best: the average absolute deviation from experimental data was 13.2 kJ/mol, i.e., less than 0.9 kJ/mol per particle. Figure 2 reports the

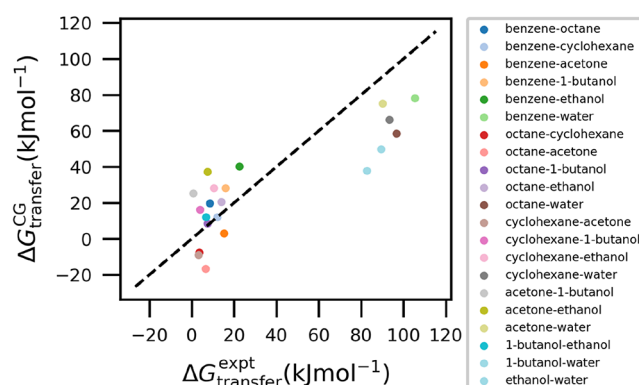


Figure 2. Partitioning of the F15 fullerene model between different pairs of solvents. Computed free energies of transfer are plotted against the experimental data.

results of the free energies of transfer for F15 with the SC5r particle type, which differs from the SC5 type only in the self-interaction (the label “r” indicates reduced self-interaction); hence, it is identical to SC5r in terms of partitioning. We notice that the F16 model, that has the best solid-state properties, also performs reasonably well in solution, with a mean unsigned error of 14.2 kJ/mol. Since both F15 and F16 models provided good agreement with experimental data both in the solid state and in solution, they were both considered in the following steps of the parametrization, while other models were discarded at this point.

Overall, our results demonstrate the expected behavior with fullerene being highly hydrophobic, as indicated by free energies of transfer between water and organic solvents. The more favorable partitioning into benzene compared with other solvents is also well reproduced. We notice that the discrepancies in partitioning between simulations and experi-

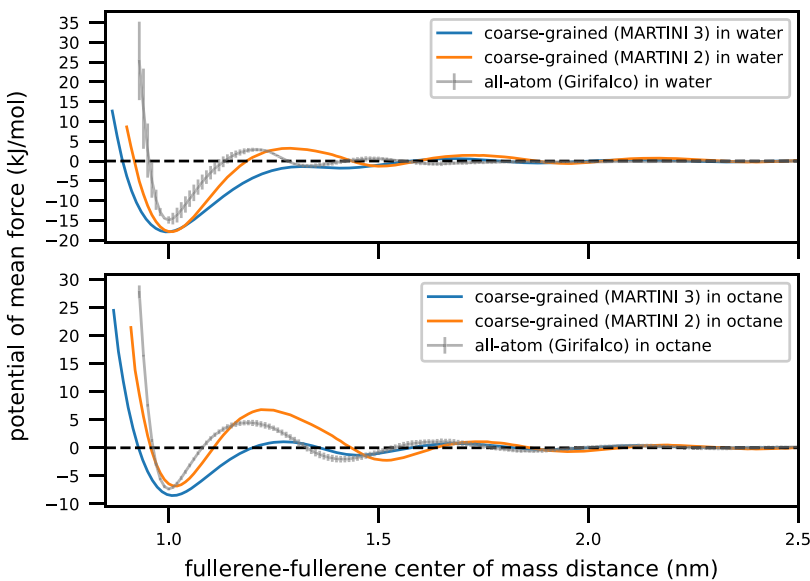


Figure 3. Potential of mean force for fullerene–fullerene interaction in water (top) and octane (bottom) for the F15 model with SC5r particle type.

ments in the Martini 3 model are larger than in Martini 2.²¹ However, in the previous model, each interaction was optimized separately, as no existing Martini 2 particle type could reproduce fullerene partitioning. The current model, instead, was obtained simply by selecting among the existing particle types, labels, and different mappings. Also, the calculation of free energies of transfer from experimental solubility data involves approximations, which can affect the reliability of the solubility-derived partitioning data, as previously noted.²¹ Finally, the solvent models have not been extensively tested; hence, the errors in partitioning could be ascribed, in principle, at least partially to the solvent models.

■ DEVELOPMENT OF THE FULLERENE MODEL: OPTIMIZATION

Since different SC5 particle subtypes (only different in the labels) have the same partitioning behavior, we used additional information to optimize the choice of nonbonded interactions, namely, fullerene–fullerene dimer potentials of mean force (PMFs) in water and octane, obtained from atomistic simulations. The PMF of dimerization provides valuable insight into the thermodynamics of aggregation, a property we wish to reproduce in large-scale simulations of fullerene in different media. Dimerization in alkanes is a proxy for aggregation in hydrophobic environments, such as the interior of biological membranes and is therefore particularly interesting when studying the interaction of fullerene with biological systems.

Here, we computed fullerene dimer PMFs in water and octane for different particle types, chosen among those providing the most accurate partitioning, and compared the results with those obtained from the atomistic model and the Martini 2 model.²¹ Again, both the F15 and the F16 models perform well, and the F15 model shows the best agreement with atomistic simulations (see Supporting Information, Figures S1–S4). In particular, F15 with the SC5e and SC5r show the strongest agreement, with SC5e performing slightly better in terms of free energy of dimerization and the SC5r performing slightly better in terms of distance at the contact minimum, which defines the geometry of the dimer. In Figure

3, we report the results for the F15 model with the SC5r particle type, finally selected as the best model.

Both the position and the depth of the first fullerene–fullerene contact minima in water are similar in all three models; the free energy at the contact minimum is slightly deeper (2.5 kJ/mol) in Martini (both versions 2 and 3) compared to the atomistic counterpart. However, in Martini 3, the dissociation barrier is significantly reduced compared to both AA and Martini 2. As for dimerization in octane, the position of the contact minimum is again very close in all three models; however, the depth of the minimum is slightly overestimated (1.5 kJ/mol), in absolute value, in the Martini 3 model; the barrier separating the first and second contact minima is also underestimated. Based on the above, we expect the Martini 3 model to show the same aggregation behavior for fullerene in water but increased aggregation in octane and other apolar media. Overall, the results for the new fullerene model are in good agreement with the previous Martini 2 model and with atomistic results, but there clearly is a margin for improvement of the new model, which would probably require optimization of individual interactions between fullerene particles and solvents.

■ FULLERENE MODEL VALIDATION: INTERACTION WITH MEMBRANES

Dimerization free energy profiles provide quantitative insight into the thermodynamics of oligomerization, while unbiased simulations allow for the study of aggregation on a larger scale. To explore the consequences of the increased fullerene–fullerene attraction in hydrophobic environments, we compared all-atom and CG simulations of fullerene aggregation in membranes. Experimental data strongly suggest that fullerene dissolves in the bilayer membrane of liposomes and does not form large aggregates.³⁶ To characterize the degree of aggregation, we calculated the fraction of monomeric fullerene during the simulations, that is a simple and unambiguous quantitative measure.¹⁹ Atomistic simulations indicate that 1-palmitoyl-2-oleoyl-sn-glycero-3-phosphocholine (POPC) membranes are more effective than octane in dissolving fullerene, and Martini models reproduce such behavior to

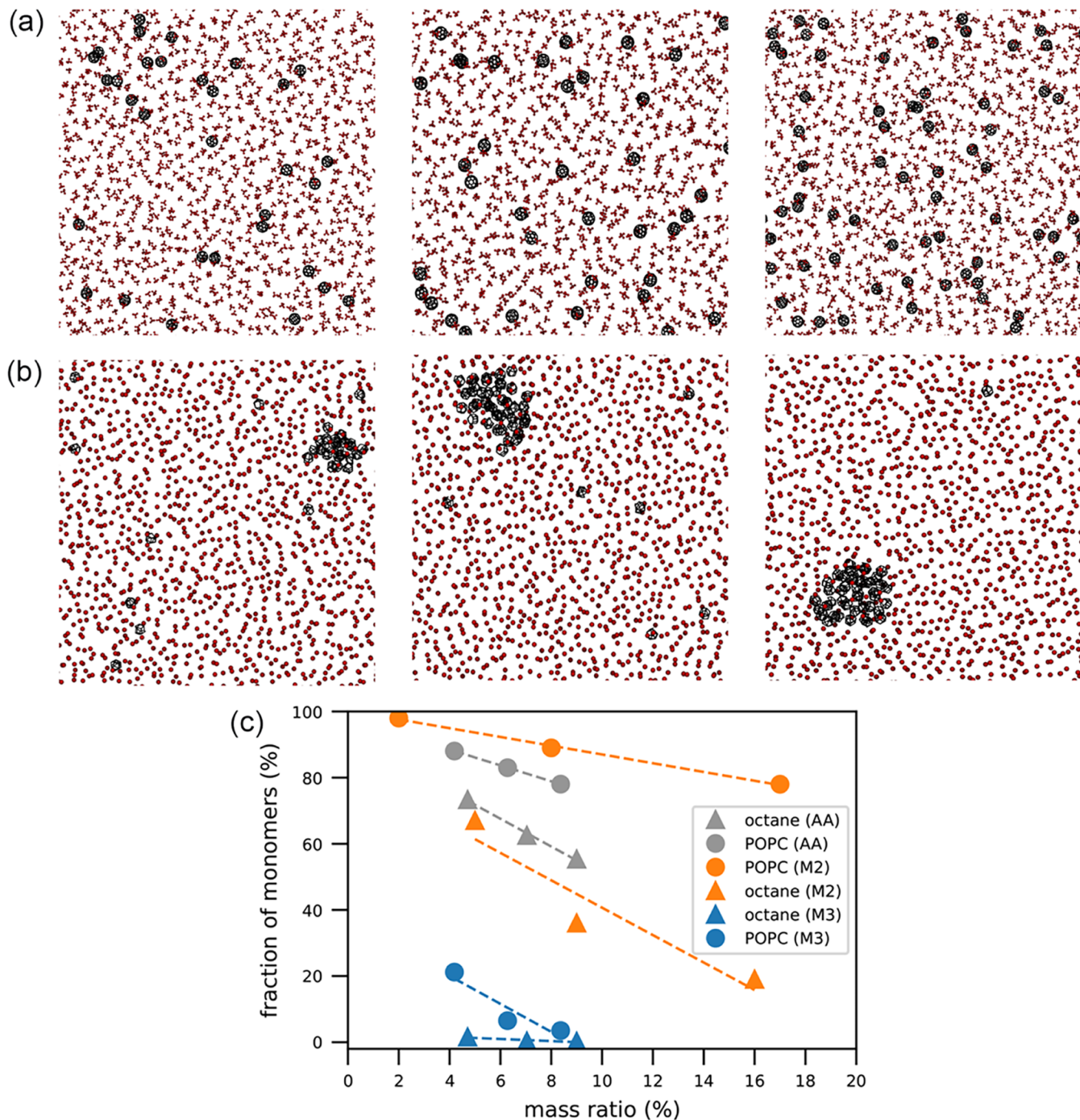


Figure 4. Snapshots of the top views at the end of the AA (a) and CG (b) simulations at different increasing fullerene concentrations (from left to right) in a POPC lipid bilayer. Water molecules are not shown for the sake of clarity. Fullerene molecules are shown in black, while the phosphate group (PO_4) is shown in red. (c) Fraction of monomeric fullerene as a function of concentration (expressed as fullerene/solvent mass ratio) in different solvents, for the all-atom (gray), the Martini 2 (orange), and the Martini 3 model (blue). For POPC, only the hydrophobic chains are taken into account. Linear regressions are displayed as visual guides only.

different extents (Figure 4). The Martini 2 model showed very limited fullerene aggregation in POPC membranes, in line with atomistic results and with a slightly higher monomer fraction.¹⁹ The Martini 3 model showed stronger fullerene aggregation and underestimated the fraction of monomer, as expected based on the PMF results (Figure 3). We notice that convergence of aggregation properties is difficult to achieve in atomistic simulations, as it requires very extensive sampling. Overall, the Martini 3 model reproduces the correct trend for

solubility in alkanes vs membranes, but there is room for improvement in terms of self-aggregation in membranes.

To further validate the new model in terms of the interaction with lipid membranes, we calculated the PMF of a single fullerene as a function of the distance from the center of a POPC membrane. This is relevant with respect to biodistribution and on environmental release of fullerenes, which poses potential health hazards, as noted in several studies.^{37–39} The hydrophobic nature of fullerenes enables them to

penetrate through biological membranes, possibly disrupting their function.¹⁵ Elucidating fullerene–membrane interaction is useful to rationalize fullerene biodistribution and its potential application in drug delivery.

We calculated PMFs for F15 models and F16 models (Martini 3) with 4 different particle types (i.e., 8 PMF calculations, see Figure 5 and Supporting Information, Figures

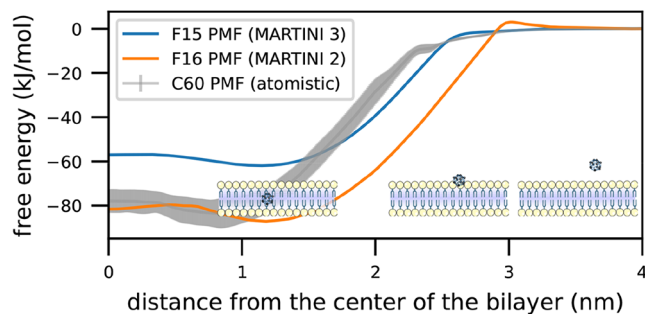


Figure 5. Potential of mean force for a system with a single fullerene and a POPC bilayer as a function of the distance between their centers of mass.

S5 and S6). All Martini 3 models underestimate the free energy gain upon fullerene permeation by about 20 kJ/mol, and differences between F15 and F16 are minor. Such underestimation indicates that the new model is less hydrophobic and interacts less favorably with the POPC membrane compared with the atomistic model and the Martini 2 model; this is in line with the results on water/octane partitioning (Figure 2). However, the overall shape of the profile is improved compared to the previous CG model, due to the absence of a barrier for penetration into the membrane. As a result, the transfer of Martini 3 fullerene from the aqueous environment to the hydrophobic interior of the POPC bilayer will be slightly faster with the new model. For both F15 and F16, the free energy minimum is in the center of the membrane for the SC5e and SC5er particle types, in contrast with all-atom results, showing that the preferred position of fullerene in a membrane should be away from the center. The models with the SC5r particle type yield a free energy minimum away from the center of the membrane, only slightly shifted compared to the atomistic simulation (1.1 nm from the center of the membrane, instead of 0.8 nm observed in all-atom simulations), and very close to the results obtained with the Martini 2 model (1.15 nm). Overall, among the many models tested in this work, the F15 model with the SC5r particle type provides the best agreement with all-atom simulations.

■ DEVELOPMENT OF THE CARBON NANOTUBE MODEL

Within the framework of the Martini 2 force field, models exist for different types of carbon nanotubes^{12,14,40} (CNTs). These

were used to understand how CNTs interact with biological membranes, which is important for biomedical applications, and also to gain a deeper understanding of the physical and chemical mechanisms underlying the potential toxicity of nanoparticles. Here we set out to update the carbon nanotube models in the framework of the Martini 3 force field. To this end, we generated starting structures and topology (ITP) files for CNTs using an updated version of the tools developed and used in previous work,²² available online at <https://github.com/bio-phys/cnt-martini>. The bond length (a in Figure 1b) was set to 0.41 nm, similar to bond lengths generally connecting small particles in Martini 3. To achieve a similar diameter as in the Martini 2 CNT model,²² we added one more particle in each CNT ring (for a total of 9 particles instead of 8). As for particle types, we used SC5 for the carbon particles by analogy with fullerene.

To confirm the quality of the choice, we calculated the partition coefficient of small CNTs between water and octanol and compared it to previous calculations by Gul et al.⁴¹ using an all-atom and a coarse-grained model, as well as to experimental results^{42,43} (Table 2). The results for the new model show excellent agreement with the experimental results: our CG model of CNT is less hydrophobic compared to both AA model⁴¹ and the previous Martini 3 model of CNT,⁴¹ and closer to experimental estimates.

■ MODEL VALIDATION: INTERACTION OF CNTS WITH LIPIDS

One of the potential applications of CNTs is as membrane porins, for applications in filtration and molecular delivery devices.^{22,44,45} Simulation studies of CNT porins were pioneered by Hummer, predicting that CNTs can efficiently conduct water.⁴⁶ Atomistic models were also used to study the interaction of CNTs with membranes,^{22,45} although the time and length scales were limited. Predictions of CNT self-aggregation and interaction with membranes require coarse-grained models that are more suitable for larger-scale studies. Hence, comparison between all-atom and coarse-grained simulations of CNTs in membranes is a relevant way to validate the performance and reliability of coarse-grained model. Here we compare atomistic and coarse-grained simulations of CNTs capped with polar groups at both ends, anchoring the ends of the CNT to the water interface, to be used as membrane porins.^{22,45} In our CG model, we used SN2 particle types for mildly polar capping groups and SP4 for strongly polar ones. The results are very similar for both SN2 and SP4 end groups, and in the following, we only report results for the SN2 group. Similar to the Martini 2 CNT tests,²² but to a lesser extent, we varied the CNTs slightly in their length and diameter (see the Methods section and Table 3). No significant trend in direct CNT-lipid interactions was found for CNTs of different sizes, and in the following, we report results only for the models with a diameter of 1.17 nm and a length of 4.26 nm.

Table 2. Computed Free Energies of a CNT(6,0) in Water, Octanol, and Partition Coefficients for AA and CG Models^a

	ΔG_{water} (kJ/mol)	$\Delta G_{\text{octanol}}$ (kJ/mol)	$\Delta G_{\text{transfer}}$ (kJ/mol)	$\log P$	$\log P^{\text{ref}}$
AA (Gul et al. ⁴¹)	-48.9 ± 0.7	-168.9 ± 0.6	-120.0	21.0	18.7, ⁴² 19.2 ⁴³
CG (Gul et al. ⁴¹)	-54.9 ± 0.0	-170.0 ± 0.0	-115.1	20.2	
CG (present work)	-24.2 ± 0.1	-130.7 ± 0.2	-106.5	18.7	

^aThe reference $\log P$ values are from refs 42 and 43.

Table 3. Properties of CNT Porin Simulations^a

funct.	diam. (nm)	length (nm)	num lipids	num water	<i>x</i> edge (nm)	<i>z</i> edge (nm)	time (μ s)
SN2	1.04	4.26	700	13,869	15.15 \pm 0.06	11.21 \pm 0.09	2.00
SN2	1.04	4.62	700	13,853	15.15 \pm 0.06	11.19 \pm 0.09	2.00
SN2	1.17	4.26	700	13,865	15.15 \pm 0.06	11.20 \pm 0.09	2.00
SN2	1.17	4.62	700	13,843	15.15 \pm 0.06	11.19 \pm 0.09	2.00
SP4	1.04	4.26	700	13,864	15.15 \pm 0.06	11.19 \pm 0.09	2.00
SP4	1.04	4.62	700	13,867	15.15 \pm 0.06	11.20 \pm 0.09	2.00
SP4	1.17	4.26	700	13,888	15.17 \pm 0.06	11.20 \pm 0.09	2.00
SP4	1.17	4.62	700	13,864	15.16 \pm 0.06	11.20 \pm 0.09	2.00

^aThe columns show (from left to right) the Martini particle type that represents the functional groups at the rim of the CNT, the CNT's length, its diameter, the number of lipids in the simulation, the number of water particles in the simulation, the average lateral dimension of the square simulation box over simulation time (with standard deviation), the average box height, and the length of the simulation.

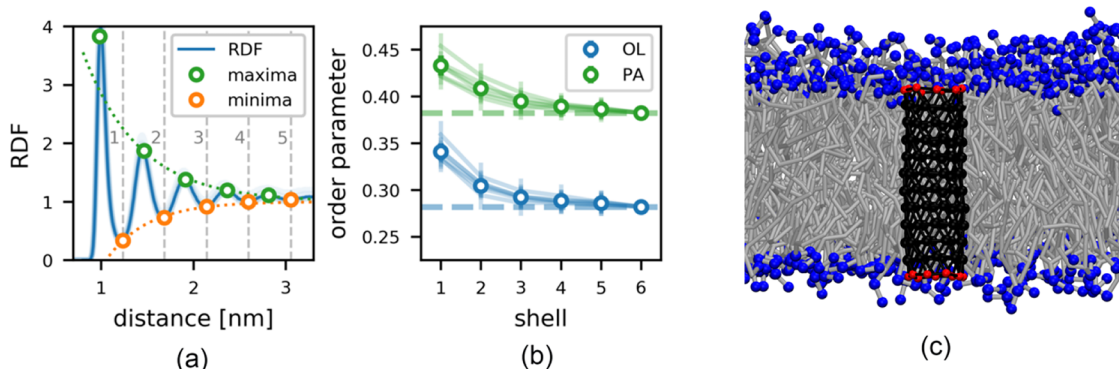


Figure 6. Lipid structure around CNT porins in simulations using the Martini 3 parameters (figure analogous to Figure 7 in ref 22). (a) Radial distribution function of POPC lipid-tail carbon particles around the main axis of a coarse-grained CNT of 4.26 nm length with SN2 end groups. Minima and maxima are marked, and the respective exponential fits are shown. Extrema below 1.1 nm were excluded from the fits. The RDFs of CNTs of different lengths are shown as faint lines. (b) Lipid order parameter S_{MARTINI} of oleoyl (OL) and palmitoyl (PA) tails in the distinct shells around a coarse-grained CNT of 4.26 nm length and with SN2 end groups. The order parameters of POPC around differently functionalized coarse-grained CNTs of the same width and different lengths are shown as faint lines. (c) Snapshot of a simulation of a CNT embedded in a POPC lipid membrane. Water is not shown for the sake of clarity.

In previous atomistic simulations, membrane lipids were shown to form a strong annular shell around the CNT when used as a porin.^{22,47} To verify that the new CG model still captures the molecular interaction of CNT with membrane lipids, we assessed the formation of annular shells of lipids when CNT is used as a membrane porin. We calculated the radial distribution function (RDF) of POPC lipid-tail particles around the main axis of CNT and with SN2 end groups and the lipid order parameter of oleoyl (OL) and palmitoyl (PA) chains in the distinct shells around a CNT and with polar end groups. The RDF (Figure 6a) shows the same features as for Martini 2, with almost perfect quantitative agreement (compared to Figure 7 in ref 22), and good agreement with atomistic simulations (Figure 3 in ref 22). Both the Martini 2 and 3 models capture the pronounced shell structure around the cylindrical CNT.

The order parameter (Figure 6b) also shows the same trend in the new and old Martini models, with an increase in the order parameter in proximity of the membrane, although such an increase is not as far-reaching as in atomistic simulations. The increase in order parameter from bulk to the first shell is slightly less pronounced for palmitoyl tails. We note that the lower baseline of the oleoyl order parameter stems from the change in POPC mapping (in ref 22, a POPC model for which the oleoyl tail was modeled with five particles instead of four). We notice that a comparison of order parameters between

atomistic and CG simulations is possible only in a qualitative way as the definitions used in each model are different.

MODEL VALIDATION: OLIGOMERIZATION OF NANOTUBES IN MEMBRANES AND WATER PERMEATION

The oligomerization behavior of carbon nanotubes in membranes was also previously assessed in simulations at the all-atom level^{22,45} It was shown that CNT dimers are stable in POPC bilayers over a time of 150 ns, when simulations start from a tightly packed dimer; analogous findings were reported for tetramers, which achieved hexagonal packing. Here, we conducted coarse-grained simulations of SN2-capped CNT dimers and tetramers embedded in POPC bilayers on time scales about 2 orders of magnitude longer. Each configuration was simulated with two initial center-to-center separations: 1.4 (closed) and 2.5 nm (far). In the case of the dimer, for both close and far dimer initial arrangements, the inter-CNT distances remained relatively stable and the CNTs maintained a parallel orientation over 10 μ s (Figure 7a). The 1.4 nm dimer maintained tight packing, partly due to strong van der Waals interactions between CNTs and partly due to lipid-mediated stabilization. The 2.5 nm dimer configuration preserved its spacing without significant drift. Lipid chain order parameters around the dimers (Figure 7b) revealed increased ordering in the first shell, particularly for oleoyl (OL) chains, consistent with results from individual CNTs (Figure 6) and with annular

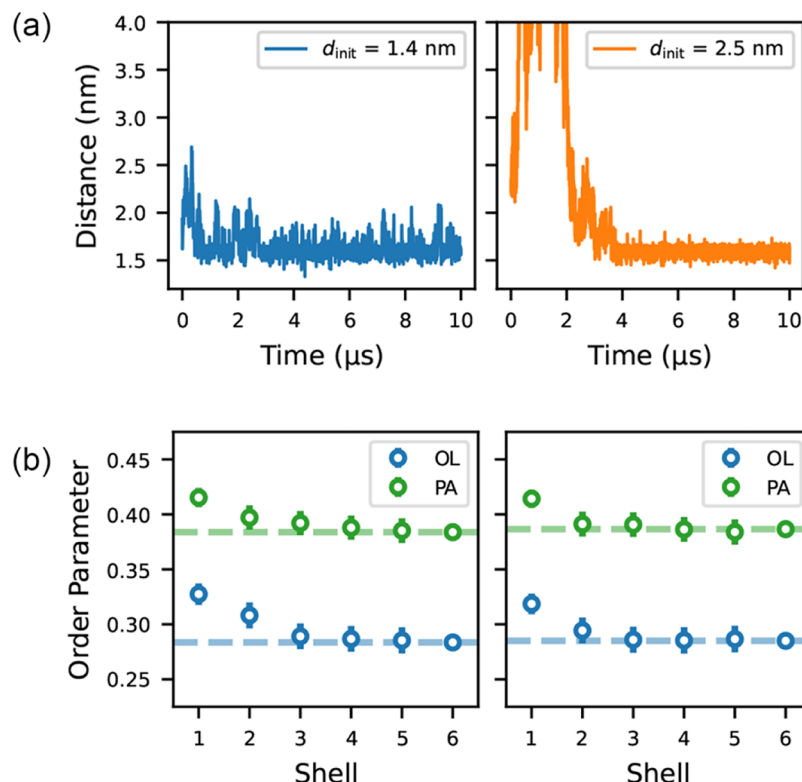


Figure 7. (a) Time evolution of the center-of geometry (COG) distance between two CNTs in dimer configurations embedded in a POPC bilayer. Two initial separations were tested: (left) close configuration (1.4 nm) and (right) far configuration (2.5 nm). Both configurations show stable spacing with minor fluctuations over $10 \mu\text{s}$. (b) Order parameters of oleoyl (OL) and palmitoyl (PA) chains of POPC lipids around CNT dimers in close (1.4 nm) (left) and far (2.5 nm) (right) configurations, computed as a function of radial shell index. Increased lipid ordering is observed in the first shell, indicating annular lipid structuring near the CNT surface.

lipid rearrangement near hydrophobic inclusions^{22,45} Both contact dimers and lipid-separated dimers showed similar ordering trends, indicating that CNT spacing has only a minor effect on the local lipid structuring.

In the case of tetramers, more pronounced structural dynamics were observed (Figure 8, top). In the close (1.4 nm) configuration, some CNT pairs remained tightly packed (e.g., CNT 2–3 and 3–4), while others fluctuated more (e.g., CNT 1–3). The far (2.5 nm) configuration showed greater separation across all CNT pairs with minimal clustering during the $10 \mu\text{s}$ trajectory. However, long time scale fluctuations in intermolecular distances show that the $10 \mu\text{s}$ time scale is insufficient for equilibrium sampling, and any further analysis should be considered with caution. Indeed, the trends for lipid order parameters suggest that the overall perturbation of the membrane remains localized and does not scale linearly with CNT number or spacing (Figure 8, bottom), but the interpretation of these results is not straightforward.

Finally, still in the context of applications of CNTs as membrane porins, we also examined water permeation through the CNTs. Atomistic simulations by Hummer⁴⁶ on CNTs of comparable diameter showed that water can permeate CNTs in a single file, and later studies with the Martini 2 model showed that water molecules can be found inside the cavity of CNTs,²² despite their size being significantly larger than for atomistic water (Martini 2 water particles represent 4 water molecules). Martini 3 features three different water models, named W, SW, and TW, with “regular”, “small”, and “tiny” size, representing 4, 3, and 2 water molecules, respectively. Here, we simulated the same CNT dimers, capped with mildly polar

SN2 groups, in POPC bilayer membranes, in the presence of water of three different sizes, and monitored water permeation during the simulations. We found that water permeated the CNT cavity in all cases, and, as expected, occupancy depended strongly on the size of the water model, with “tiny” water entering CNTs more easily (Figure 9). These results suggest that our new CG model can potentially be used in studies on water permeation through CNT porins. However, it should be noticed that simulations with “tiny” water are significantly more expensive, as the number of particles is about twice the number necessary for the same volume of “regular” water. Also, any effects related to water hydrogen bonding and electrostatics (e.g., the specific orientation of water molecules observed in atomistic simulations) are lost in our CG simulations; hence, special caution should be used when interpreting water permeation results. We also note that the use of water phases made up fully of “small” and “tiny” water beads is not recommended as they were not thoroughly tested.³⁰

■ DEVELOPMENT OF THE GRAPHENE MODEL: MAPPING

Previously, three Martini 2 models for graphene were published and used to study the interaction of graphene with lipids^{26,48} and with water.²⁷ Here, we set out to develop a Martini model of graphene compatible with version 3 of the force field.

The first challenge in devising a Martini 3 model for graphene is the mapping. We tested a number of different mappings for graphene molecules with different symmetries

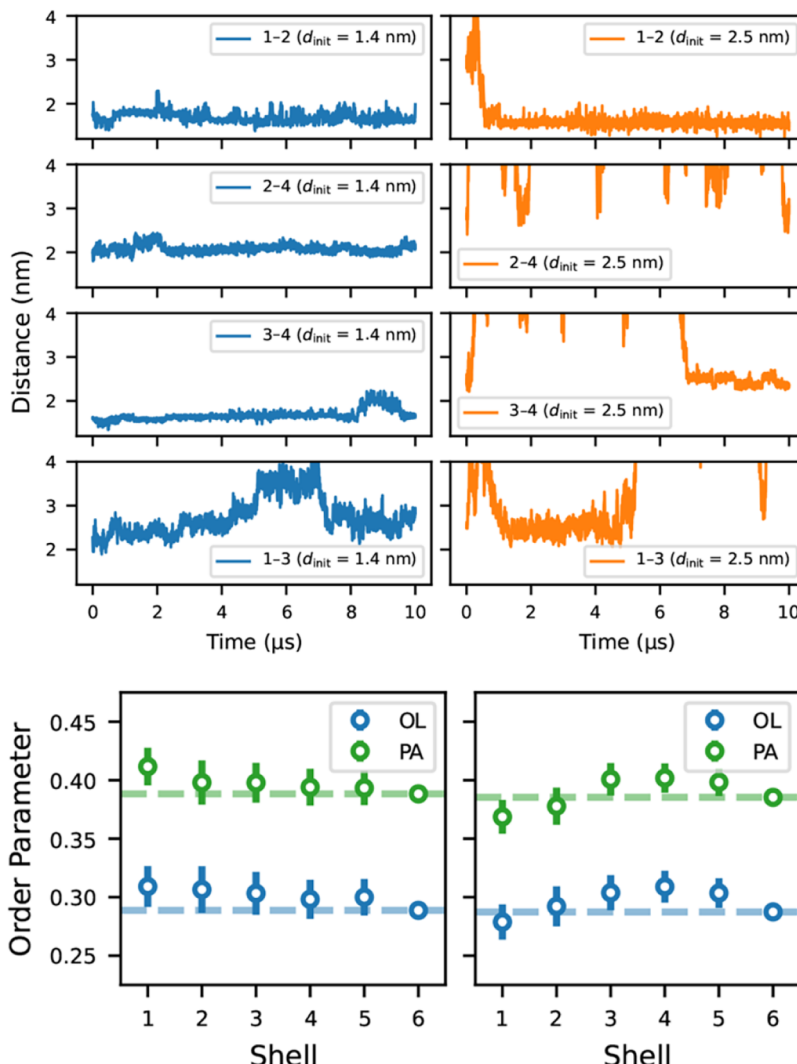


Figure 8. (Top) Time evolution of inter-CNT distances for all pairs within a CNT quartet embedded in a POPC membrane. Simulations were initialized with either (left) close (1.4 nm) or (right) far (2.5 nm) spacing between the central axes. Close-packed CNTs maintain tighter clustering, while far-separated CNTs remain more dispersed. (Bottom) Order parameters of oleoyl (OL) and palmitoyl (PA) chains of POPC lipids surrounding CNT quartets. Data are shown for both initial configurations: close (1.4 nm) (left) and far (2.5 nm) (right). Localized increases in lipid ordering are observed, with slightly higher order in the close-packed arrangement.

and different particle sizes. We chose to use tiny particles (T types) for graphene, despite the branching in atomistic structures, which would allow models with less CG particles, because the planar aromatic structures are best described by tiny particles, particularly in terms of stacking interactions.³⁵ In terms of symmetry, we settled on hexagonal symmetry, replicating the symmetry of the original molecule. Notice that each carbon atom in the hexagon of the all-atom model contributes 1/3 to the CG particle; therefore, our choice corresponds to a 2-to-1 mapping. One possible drawback of our choice is that the mapping of the model does not follow the same scheme used for small aromatic molecules;³⁵ in the case of graphene, the edges are under-mapped (Figure 10), therefore the molecular volume is underestimated. Such an effect is noticeable in the case of extremely small graphene sheets, i.e., large aromatic carbon molecules, for which our mapping scheme is not ideal. Nevertheless, graphene sheets with realistic size are large enough (tens of nanometers or larger) that the effect of undermapping (and underestimating the molecular volume) is negligible, and none in the case of

infinite, periodic sheets. On the other hand, there are two clear benefits resulting from hexagonal symmetry: first, a more realistic representation of molecular properties, i.e., the interaction with liquids and other species; second, the simplicity in the choice of virtual sites, which greatly increase numerical stability.

The molecular structure of graphene is very rigid, with a high Young's modulus (about 1 TPa⁴⁹). Therefore, we anticipate that a realistic graphene model needs very stiff bonds; this generally poses problems for numerical stability in MD simulations. Indeed, a previous CG model of graphene⁵⁰ used an extremely high force constant for bonded parameters to reproduce graphene mechanical properties, which imposed a time-step limit of 4 fs to achieve numerical stability. A solution for this issue is the use of virtual sites, i.e., mass-less particles whose position is calculated as a function of other particle positions.⁵¹ The virtual site approach increases the numerical stability of the model, as it reduces the number of necessary bonds of the model and increases the masses of the real particles. Following this approach, we selected the particles at

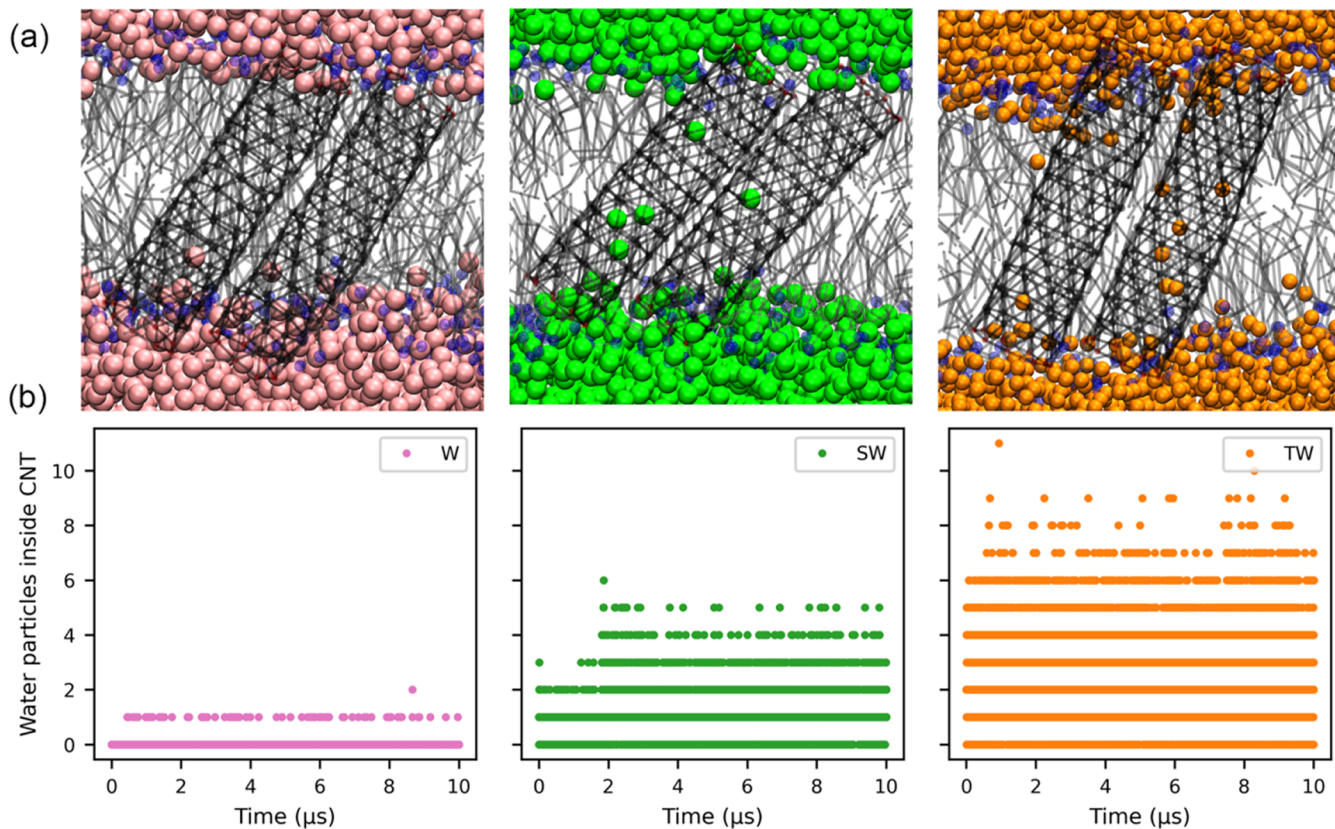


Figure 9. (a) Snapshots of CNT dimers in a POPC membrane with water of “regular” size (pink, left panel), “small” size (green, middle panel), and “tiny” size (orange, right panel). (b) Number of water particles inside the CNT as a function of simulation time; colors match the ones used in (a).

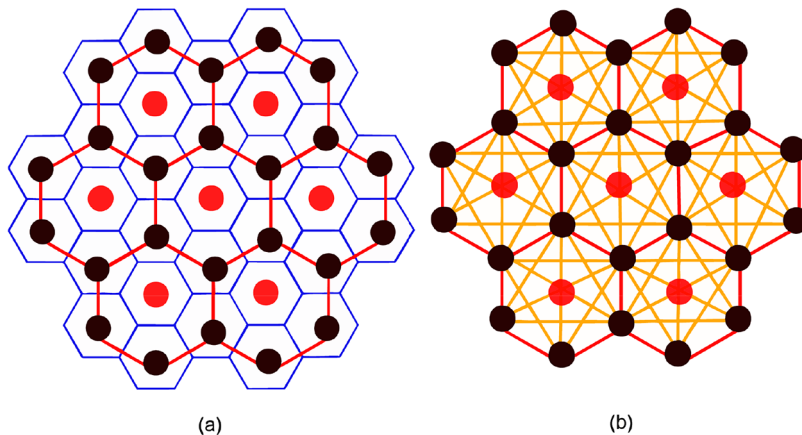


Figure 10. (a) CG mapping of graphene parametrized in this work. The atomistic structure is shown in thin blue lines, while the CG structure is in spheres, with virtual particles (red) and real particles (black). Harmonic bonds are represented in red. (b) CG model of graphene. Harmonic bonds are represented in red, with real (black) and virtual (red) particles shown as spheres. Harmonic bonds are defined only between real particles, and no harmonic bonds involve virtual sites (full details are given in Figure S8). Besides bonds following the hexagonal geometry, additional bonds (orange lines) connect particles within each hexagonal frame in order to achieve higher rigidity.

the center of each CG hexagon as virtual sites (colored in red in Figure 10a). Nonbonded interactions between the virtual site and the corresponding neighboring particles were excluded. The hexagonal symmetry is not altered by the placement of virtual particles at the geometric center of the hexagonal frame.

■ DEVELOPMENT OF THE GRAPHENE MODEL: BONDED AND NONBONDED INTERACTIONS

An initial guess for bonded parameters was obtained from AA simulations of graphene in a vacuum. We did not include angle potentials in the model, but we included improper dihedrals in order to keep the molecule flat; the force constant was derived from the AA simulation. Using the initial guess based on AA simulations, we calculated the Young’s modulus (E) as the slope of the linear fit to the stress-strain plot (see the **Methods** section). The value initially obtained was much lower than the

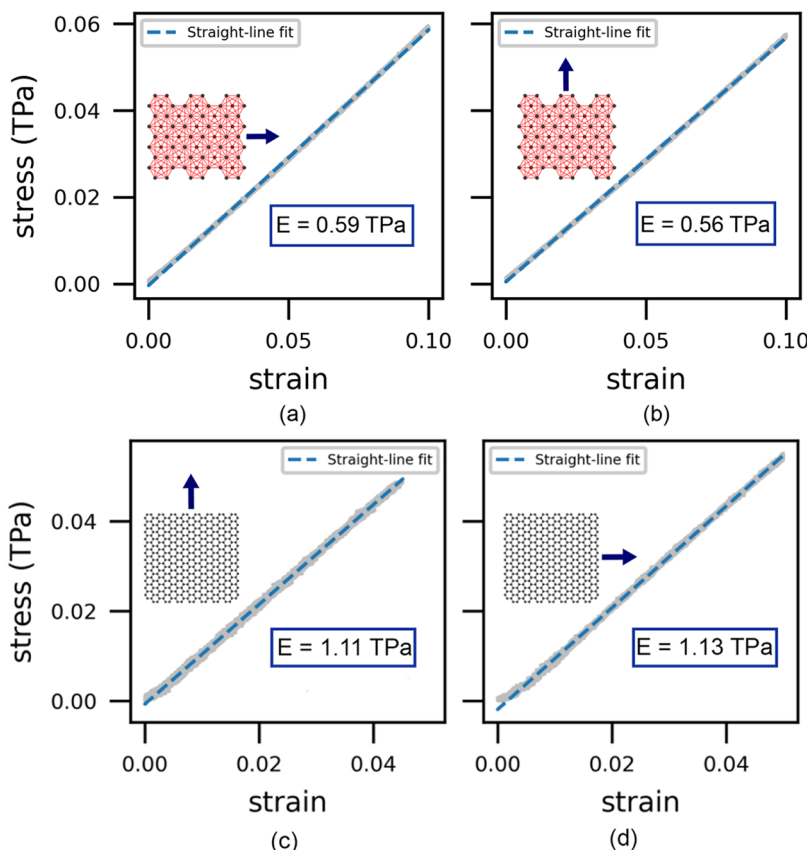


Figure 11. Stress vs strain curves and linear fits, calculated on a single graphene sheet, with the stress applied in (a) zigzag and (b) armchair directions for the CG model, (c) armchair and (d) zigzag for the AA model. The Young's modulus (E) is obtained from a linear fit.

experimental value of 1.0 TPa.⁴⁹ To increase mechanical strength, two strategies are available: to increase the force constant of the bonds or to increase the number of bonds (or both). Increasing the force constant caused numerical instability with the standard Martini time step of 20 fs, so we resorted to adding extra bonds to the model (shown in Figure 10b; more details in Supporting Information S5 and Figure S7). The parameters were finally chosen (Table S9 in Supporting Information) yielding a Young's modulus I of 0.59 ± 0.04 TPa along the zigzag direction, and 0.56 ± 0.01 TPa along the armchair direction (Figure 11a,b). These values are about 30–35% lower than the experimental value. Higher values of Young's modulus could be obtained by increasing the force constant of all bonds to reach a value of 50,000 kJ/mol nm², but this required reducing the time step from 20 to 14 fs to achieve comparable numerical stability (see Supporting Information S6 and Figure S8). Here, we prefer to propose a model that is a compromise with sufficiently high stiffness and high numerical stability, usable with a time step of 20 fs.

We notice that, independent of the chosen value of the bond force constant, graphene gives slightly different values of the Young's modulus depending on the direction of application of stress. This is expected due to the symmetry properties of the molecule. To confirm this, we computed the Young's modulus for the AA model and found indeed values of 1.11 ± 0.06 TPa along the armchair direction, and 1.13 ± 0.05 TPa along the zigzag direction, i.e., the Young's modulus is indeed higher in the zigzag direction compared to the armchair direction; this aligns well with previous findings,^{50,52} and confirms that the ranking of the two moduli is an intrinsic property of their

topologies. However, we notice that, due to the mapping used in our CG model, the armchair and zigzag orientations are exchanged compared to the atomistic representation; hence, the ranking of the two moduli is actually reversed.

As for nonbonded interactions, we chose the standard TC5 particle type of the Martini 3 force field, i.e., the particle type used for 2-1 conjugated carbon-based systems; this is similar to the choice made for fullerene and carbon nanotubes, using the SC5 particle type. Both SC5 and TC5 provide excellent agreement with experimental free energies of transfer of aromatics.³⁵ In the case of fullerene and nanotubes, the use of a larger particle (size S) reduces the computational cost (3:1 mapping instead of 2:1). In the case of graphene, choosing SC5 leads to incorrect spacing among graphene sheets piled up in larger graphitic structures (e.g., carbon dots), while the TC5 particle type yields correct interleaflet spacing.

Based on the parametrization described above, we developed code (freely available at <https://github.com/MoMS-MMSB/Martini3-Graphene>) to generate structures and topologies (for the Gromacs⁵³ software package) for both finite and periodic graphene sheets of any (user-defined) size.

GRAPHENE PERIODIC MODEL

Many applications of graphene (such as mechanical stretching and interaction with other materials) require simulating sheets that are much larger than the typical simulation box, even at the CG level. One possible solution would be to use a periodic CG model of graphene, allowing for seamless representation of an infinite sheet and avoiding edge effects that could otherwise distort the system properties. Here, we developed a periodic

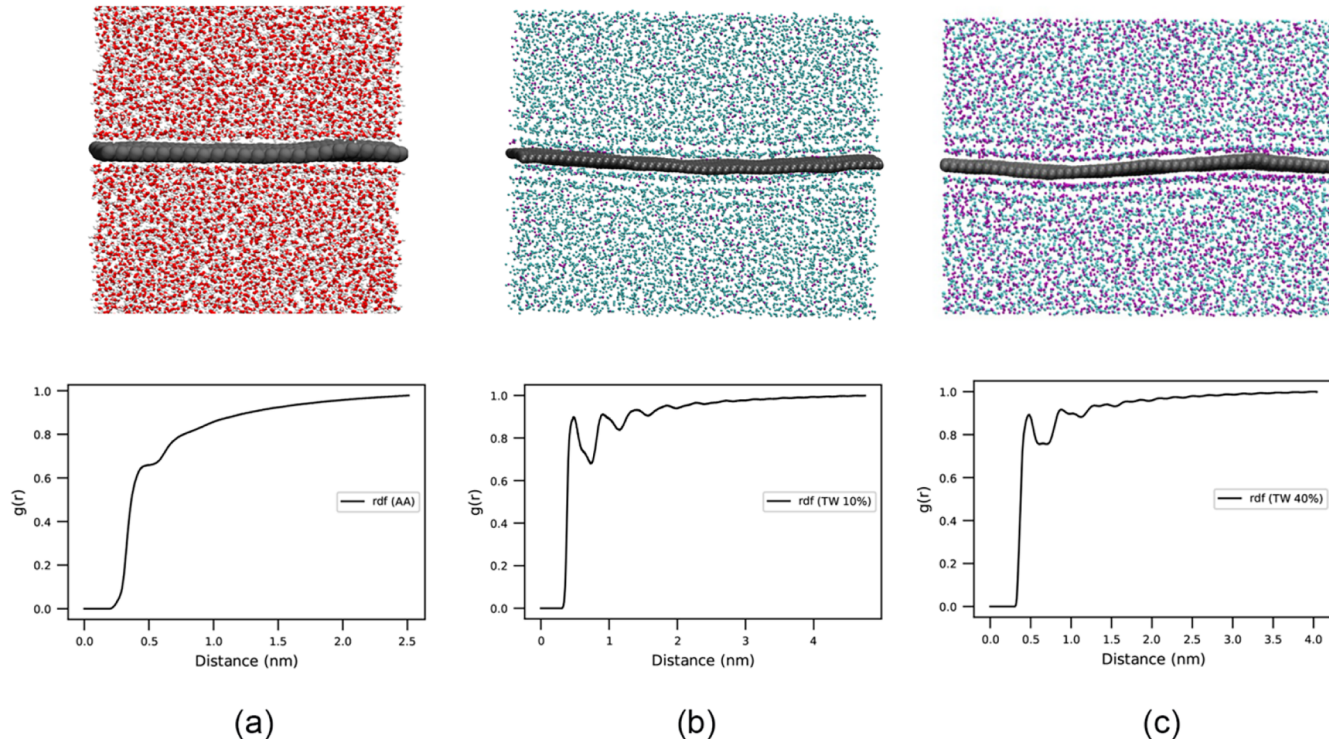


Figure 12. Snapshots at the end of the simulation (top panels) and radial distribution function (RDF) of water with graphene as a reference in (a) AA simulations, (b) CG simulations with 90% regular water beads and 10% tiny water beads, and (c) CG simulations with 60% regular water beads and 40% tiny water beads.

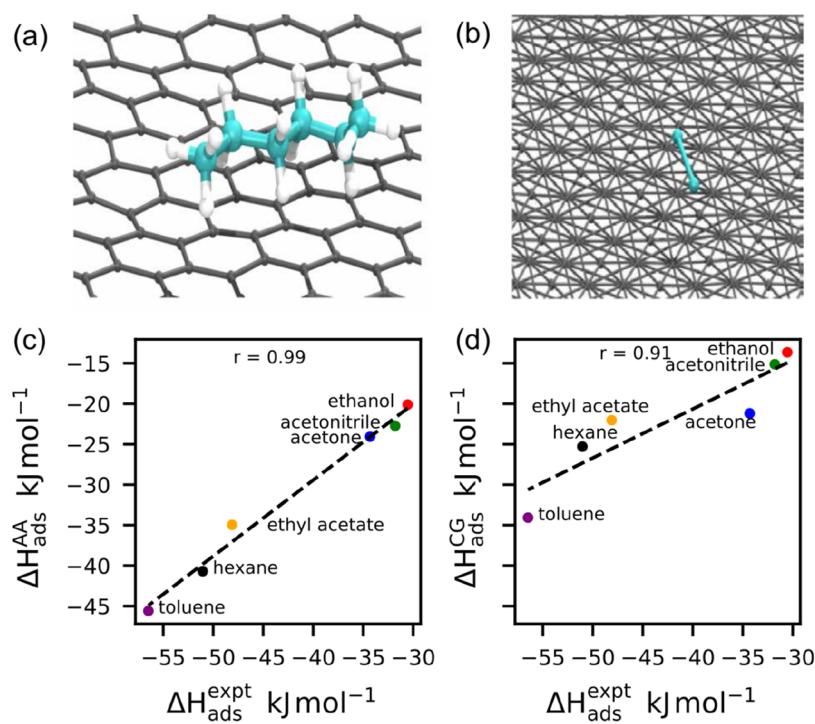


Figure 13. Adsorption of hexane onto (a) the AA model of graphene and (b) the CG model of graphene. Computed adsorption enthalpy from (c) AA simulations against experimental data and (d) CG simulations against experimental data.

CG model of graphene by defining the bonded interactions (bonds, angles, and improper dihedrals) such that a CG particle at the edge of the simulation box is connected to a particle on the opposite side (due to periodic boundary conditions). In gromacs, this requires that the dimensions of

the simulation box be defined very precisely to be compatible with the periodicity of the CG lattice. Given the anisotropic nature of graphene, anisotropic pressure coupling must be applied in all of the simulations of periodic molecules. Further

details on the simulation parameters used for the periodic CG model of graphene are given in *Supporting Information S7*.

In simulations of periodic graphene molecules, translational and rotational motion are restricted due to periodicity, which makes the system very similar to a solid, perfectly planar surface. The challenges in modeling solid–liquid interfaces using Martini 3 have already been described by Cambiaso et al.⁵⁴ They observed that regular Martini water beads form unrealistically ordered (layered) structures near smooth planar surfaces, potentially leading to water freezing. Indeed, we found similar effects in simulations of periodic graphene molecules: water layering was strongly enhanced in simulations with regular Martini water, an effect not observed in AA simulations (**Figure 12a**). In order to mitigate the layering artifacts, we followed the suggestions by Cambiaso et al.⁵⁴ and mixed water beads of regular size with water beads of tiny size, in different proportions. We observed that the mixtures with tiny water beads significantly reduced the layering artifact; the reduction was already evident with 10% of tiny water beads and stronger with 40% of tiny water beads in the water mixture (**Figure 12c**). However, some layering persisted in all simulations with periodic CG graphene models.

■ GRAPHENE MODEL: VALIDATION

As stated above, graphene was built with TCS particles, as they are generally used, in Martini 3, to represent aromatic hydrocarbons. To validate such a choice, we calculated the enthalpy of adsorption for a number of small molecules on the graphene surface; these results were then compared to both atomistic simulations and experimental measures when available. This validation is relevant, for instance, for the case of graphene-based chemical detectors, able to detect different molecular species adsorbing or desorbing from the surface.⁵⁵ We calculated the enthalpy of adsorption for six organic molecules: acetone, acetonitrile, ethanol, ethyl acetate, hexane, and toluene, already available in the standard Martini 3 database.^{35,56} The adsorption of one of the molecules, hexane, in the AA and CG models of graphene is shown in **Figure 13**.

Figure 13c,d shows the correlation between simulations and experiments for both AA and CG models. Both models underestimate the enthalpies of adsorption measured in experiments,⁵⁷ to a different extent—the CG model showing larger discrepancies. The underestimate can be ascribed to several factors: first, Martini is parametrized against free energy of transfer between different solvents¹⁷ and other quantities related to free energies (e.g., miscibilities). While it reproduces well free energies, it is known not to reproduce accurately enthalpies,¹⁷ due to the reduced entropy contribution in the CG representation. While quantitative agreement is out of reach for both atomistic and CG models, the correlation between simulations and experiments is excellent in the case of atomistic simulations (correlation coefficient of 0.99) and still strong (correlation coefficient of 0.91) in the case of CG simulations. Most importantly, the CG model reproduces the same trend observed in the experiments.⁵⁷ In conclusion, our model can be used, despite its limitations, to provide semiquantitative estimates of interaction energies of organic molecules with graphene and can clearly distinguish between weakly and strongly adsorbed molecules. If new experimental free energy data become available, comparisons could better demonstrate the accuracy of the Martini graphene models.

■ DISCUSSION

Here, we developed new coarse-grained models for three carbon nanomaterials, namely, C₆₀ fullerene, single-walled carbon nanotubes, and graphene. These are among the most widely used carbon nanomaterials, and all models are made freely available to the wide nanoscience and nanotechnology communities.

The models are compatible with the latest iteration of the Martini force field, Martini 3, and feature a consistent use of the Martini particle type C5, which is the same used for aromatic hydrocarbons. Despite the consistent choice of particle type, each model shows a different level of accuracy in reproducing the target properties selected here. The model of fullerene has increased accuracy in terms of solid-state properties with the lattice constant close to its experimental value,³¹ but does not perform as well as its predecessor^{15,21} in terms of partitioning between different solvents. In version 2 of the Martini force field, the introduction of a custom particle for fullerene was necessary because no existing particle type could reproduce partitioning data to a satisfactory extent. The development of a custom particle allowed fitting many interactions based on available experimental solubility data but also required numerous trial-and-error calculations to determine the values of LJ interactions with different solvents, which was very time-consuming. Such fine-tuning of individual interactions should no longer be necessary with version 3 of the force field, thanks to a much more extensive coverage of chemical space; 843 particle types exist in Martini 3. That said, the development of new particles has become more challenging in the new version because a very large number of interactions need to be set. Therefore, our optimization focused on the choice of exact mapping and the choice among the available particle types. The nonoptimal results obtained for fullerene partitioning point to a possible need to refine the Martini 3 interaction matrix or recognize the specific chemical nature of fullerene by introducing a more specific particle type. However, this need should be considered with caution, as some uncertainty remains on the accuracy of experimental solubility data for fullerene (which lack reported error bars) and fullerene atomistic simulations, which may be affected by both convergence and accuracy issues. Nonetheless, the current Martini 3 model provides a reasonable approximation for fullerene properties, with room for improvement, in particular regarding the overly strong aggregation of fullerenes in a lipid membrane environment.

The new CNT model reproduces key interactions with lipid membranes, which are crucial for understanding their behavior in biological systems and for potential applications in nanotechnology. The model accurately captures the formation of an annular lipid shell around the CNT when it is used as a membrane porin, as highlighted by the radial distribution function of POPC lipid chains. This structural feature is consistent with previous all-atom simulations and with the Martini 2 model,²² indicating that the new model preserves essential molecular-level interactions. The lipid order parameters calculated for oleoyl and palmitoyl chains in the vicinity of the CNT show an increase in the order near the nanotube surface. While this trend aligns with atomistic simulations, the effect is less pronounced in the Martini 3 model. This slight discrepancy may be ascribed to the coarse-grained nature of the model, which cannot fully resolve the fine details captured in atomistic simulations. The model's performance remains

consistent across different CNT lengths and end-group polarities, suggesting its robustness and versatility for various CNT configurations. This adaptability is particularly valuable for studying CNTs in diverse environments and applications. The Martini 3 CNT model also reproduces the stability of CNT assemblies in membranes, which validates its suitability for studying CNT aggregation and cooperative effects in membrane-mediated contexts. Finally, water enters CNTs when they function as membrane porins, similar to the behavior of all-atom models and the previous Martini 2 model,²² again corroborating the new model.

A previous Martini 3 model of CNTs exists,⁴¹ employing the same chemical type (“C5”) but using a higher resolution representation with tiny (T) beads instead of the small (S) beads applied in this work. The model was developed to study pristine CNTs and their functionalization with polystyrene (PS) and carboxyl-terminated polystyrene (PS-COOH), with a focus on how polymer chain length and grafting density influence CNT interactions with lipid bilayers, particularly in drug delivery applications. Given the consistent choice of the chemical type, significant differences in accuracy are not expected. However, the present implementation offers greater flexibility in constructing structures of varying sizes. A systematic comparison of the two models is beyond the scope of this work, but would be valuable for assessing their respective strengths and limitations.

A previous Martini model of graphene⁴⁸ reproduced mechanical properties accurately, particularly the very high Young’s modulus. The model presented here features a lower rigidity, with a Young’s modulus about 40% lower than the experimental value. The same model can be easily modified to reach the experimental rigidity by increasing the value of force constant for all bonds. The model with a higher force constant requires an integration time step of 14 fs, as opposed to the time step of 20 fs generally used in Martini MD simulations. A model with the correct rigidity may be useful in specific applications of graphene when it is important to reproduce elastic properties accurately. However, graphene sheets are unlikely to experience significant stretching or compression during their interaction with biological or environmental components and in most other practical applications. For this reason, we believe our “standard” model will be of interest to most users, preferring high computational efficiency and full compatibility with other components of the Martini force field.

The mapping of the graphene model employed in this work does not follow the standard methodology applied to small molecules,³⁵ for two reasons: first, graphene is not a small molecule, and a CG model needs the capability of representing very large sheets, approaching the size of realistic graphene sheets, or even infinite (periodic) sheets. Indeed, here we developed code to build models for both finite (nonperiodic) and infinite (periodic) sheets. In the case of finite molecules, the edges are under-mapped, meaning that the atoms at the edges are not fully mapped into the corresponding particles. However, as the size of the sheet becomes larger, the effect of edges becomes less relevant. In the case of infinite periodic molecules, the issue disappears. Another reason why graphene requires a distinct mapping approach is the need to retain its hexagonal symmetry, which is paramount in the representation of interactions with other species. For these reasons, we consider the present model as a significant advancement over previous Martini models of graphene.^{26,27,48}

CONCLUSIONS

Here, we developed new CG models for fullerene, carbon nanotubes, and graphene compatible with the Martini 3 framework. The new models allow leveraging the enhanced capabilities offered by the latest iteration of the force field and allow the study of CNM interactions across a wide spectrum of systems, enabling more comprehensive investigations on their behavior and potential impact. The new models avoid the need for custom particles that were necessary in Martini 2, while maintaining a reasonable performance. The model of fullerene reproduces properties of both the solid state and solutions. The model for CNT can reproduce the interactions with membranes observed with atomistic simulations and version 2 of the force field, for instance, when used as a porin spanning lipid membranes. The model for graphene can reproduce trends in the adsorption enthalpies of organic molecules with different polarities, enabling the study of a wide range of processes at molecular resolution. Overall, our new models pave the way to the development of accurate models of functionalized carbon nanomaterials, e.g., fullerenols, functionalized CNTs, and graphene oxide, and enable large-scale simulations of carbon nanomaterials with the vast spectrum of biomolecules and materials already available in the Martini force field.

METHODS

Atomistic Simulation Parameters. Lennard-Jones (LJ) parameters for the atomistic model of fullerene were taken from the work by Girifalco,³² and were tested in previous works.^{21,22} Bond lengths were taken from experimental NMR data,⁵⁸ and the bonded force constants were taken from optimized potentials for liquid simulation (OPLS)-AA force field⁵⁹ (carbon–carbon bond in aromatics). Partial charges on all atoms were set to zero. The force field for all organic solvents was OPLS-UA.⁶⁰ Parameters for the lipids were taken from the work of Berger et al.;⁶¹ the water model was SPC.⁶² All simulations of condensed phases used a cutoff of 1.0 nm for nonbonded interactions, with the particle mesh Ewald method used for long-range electrostatics.⁶³ We used the stochastic integrator in all calculations with an inverse friction coefficient of 1 ps.

For atomistic simulations of CNT porins in lipid bilayers, we used the Lipid 14 force field⁶⁴ in Amber 14⁶⁵ for lipids, and derived GAFF-style^{66,67} models for the different functionalized CNTs. The water molecules were modeled using the TIP3P model with the ionic concentration of 150 mM NaCl.

The CHARMM36 force field⁶⁸ was used in all-atom simulations of graphene. The electrostatic interactions were modeled by using the particle mesh Ewald method^{69,70} with a cutoff set to 1.1 nm, while Lennard-Jones (LJ) potentials were switched off smoothly between 1.0 and 1.2 nm. Hydrogen bonds were constrained. LINCS algorithm⁷¹ was used to constrain all covalent bonds involving hydrogen atoms.

All atomistic simulations were performed with the GROMACS software⁵³ (version 2022.4) with a time step of 2 fs. The temperature was maintained close to the reference value by applying V-rescale thermostat,⁷² whereas for constant pressure, the Parrinello–Rahman barostat⁷³ was used with a time constant of 5.0 ps and a compressibility of 4.5×10^{-5} bar⁻¹.

CG Simulation Parameters. Simulation parameters were the standard ones used with the Martini force field.

Nonbonded interactions were calculated with a cutoff of 1.1 nm. A shift function was applied for electrostatic interactions from 0 nm and for LJ interactions from 0.9 nm. Electrostatic interactions were scaled with a dielectric constant of 15. All simulations in the NPT ensemble were carried out at 310 K, using the leapfrog integrator,⁷⁴ the c-rescale barostat⁷⁵ (time constant of 8 ps, compressibility of 3×10^{-4} bar⁻¹). All CG simulations were performed with the GROMACS software⁵³ (version 2022.4) with a time step of 20 fs.

CG Simulations: Enthalpy of Sublimation. In simulations, we calculated the enthalpy of sublimation (ΔH_{sub}) using

$$\Delta H_{\text{sub}} \approx U_{\text{gas}} - U_{\text{solid}} + RT \quad (1)$$

where U_{gas} and U_{solid} are the total energies (per mole) of the gas and solid phase, respectively, R is the universal gas constant, and T is the absolute temperature. For simulations of a solid, we built face-centered cubic (FCC) fullerene crystals with the experimental lattice constant of 1.417 nm³¹ and simulated the crystals for 10 μ s in the NPT ensemble (temperature of 298 K, pressure of 1 bar, compressibility of 3.4×10^{-4} bar⁻¹, isotropic pressure coupling). Simulations in the gas phase were performed in the NVT ensemble (298 K) with the stochastic integrator (with an inverse friction coefficient of 1 ps), using a single fullerene molecule in a large empty box (10 \times 10 \times 10 nm³).

CG Simulations: Free Energy of Transfer. The free energies of transfer between different solvents were computed with the thermodynamic integration (TI) method.⁷⁶ A series of 30 simulations with unequally spaced λ points going from 0 to 1 were performed using the stochastic dynamics integrator (inverse friction coefficient of 1 ps). Each simulation was equilibrated for 10 ns, and the production runs were 200 ns long. A soft-core potential, with the soft-core parameter α set to 1.3, soft-core λ power to 1, and the range of the interaction (soft-core σ) to 0.47 nm, was used to avoid the singularity in the potential when interactions were switched off.²¹ The free energies and corresponding errors were finally computed using the multistate Bennett acceptance ratio (MBAR).⁷⁷

CG Simulations: Potential of Mean Force. The potential of mean force (PMF) was calculated for fullerene dimers in both octane and water using the umbrella sampling (US) technique.⁷⁸ In a series of simulations, two fullerene molecules were restrained at a given distance from one another, between 0.9 and 2.9 nm with 0.1 nm increments, using a harmonic potential (force constant of 1000 kJ/mol nm²). Simulations for each US window were performed for 10 μ s in the NPT ensemble at 313 K with isotropic pressure coupling (1 bar).

The PMF of fullerene as a function of the distance from the center of a POPC lipid bilayer was also computed by using the same methodology. The simulation box contained one fullerene molecule, 128 POPC lipids (64 per leaflet), and 1500 water molecules. The distance between the center of mass (COM) of fullerene relative to the POPC bilayer along the bilayer normal (z) was used as the reaction coordinate for umbrella sampling simulations; only the lipid particles within a cylinder of radius 1.5 nm around the fullerene molecule were used to compute the bilayer COM. Distances were restrained with a harmonic potential (force constant: 1500 kJ/mol nm²) between 0 and 4.5 nm with 0.1 nm increments. Each US window was simulated for 10 μ s, and the first 1 μ s was removed from the analysis. We applied semi-isotropic pressure

coupling with the c-rescale barostat⁷⁵ (time constant of 8 ps). PMFs were constructed using WHAM.^{79,80} The statistical uncertainty in all US simulations was evaluated using the bootstrap analysis as implemented in GROMACS (gmx wham).⁸⁰

Aggregation: Fraction of Monomeric Fullerene in Octane and POPC Membrane. Unbiased MD simulations of fullerene in octane and the POPC membrane were performed to characterize its aggregation behavior at the same temperature, at different concentrations. All simulations started with monomeric fullerene placed on regular grids. We assessed the degree of aggregation of fullerene on the basis of the fraction of fullerene that remains monomeric during the simulations.¹⁹ AA simulations were performed for 9 μ s, while the CG simulations were performed for 40 μ s.

CG Simulations: Free Energy of Transfer and Partition Coefficient of a CNT. For the free energy of transfer between octanol and water, a small CNT with (6,0) chirality and an approximate length of 1.5 nm was used. The free energy of solvation in both solvents was computed by using the TI method. A series of 30 simulations with unequally spaced λ values ranging from 0 to 1 were performed by using the stochastic dynamics integrator with an inverse friction coefficient of 1 ps. Each simulation was equilibrated for 10 ns, followed by a 200 ns production run. Soft-core potentials were applied with the soft-core parameter α set to 0.5, and soft-core λ power set to 1. Temperature was set to 298 K. Finally, the partition coefficient, represented by $\log P$, proportional to the free energy of transfer between two immiscible solvents—water and octanol—was computed using

$$\log P = \frac{-\Delta G_{\text{transfer}}}{RT \ln(10)} = \frac{-(\Delta G_{\text{octanol}} - \Delta G_{\text{water}})}{RT \ln(10)} \quad (2)$$

where R is the universal gas constant and T is the absolute temperature.

CG Simulations: Simulation of CNT Porin in the Lipid Membrane. Membrane simulations of 8 slightly different CNT porins (Table 3) were set up using insane.py⁸¹ and run using Gromacs 4.6.5^{82,83} following the same protocol as in ref 22.

CG Simulations: Determination of Graphene Mechanical Properties. The tensile response of the graphene model was measured by performing a steered molecular dynamics (SMD) simulations. One end of a nonperiodic equilibrated structure was pulled along the X or Y direction at a pull rate of 0.002 nm/ps, while keeping the opposite end fixed. The strain was then calculated as the ratio of extension and length of the graphene sheet along the dimension parallel to the pulling. Similarly, the stress is calculated as the ratio of the applied force and the cross-sectional area. Finally, the Young's modulus was obtained as the slope of the linear fit to the stress-strain curve.

CG Simulations: Enthalpy of Adsorption. To calculate the enthalpy of adsorption of small molecules onto the graphene surface, each molecule was randomly placed inside the simulation box (21 \times 18 \times 20 nm³) with a CG model of a periodic graphene nanosheet. Then, NVT molecular dynamics simulations were performed using the stochastic dynamics integrator (inverse friction coefficient of 1 ps) for 10 μ s at a constant temperature (323 K). From NVT simulations, the interaction energy ΔU between graphene and the adsorbed molecule was calculated and averaged over all configurations

representing the adsorbed state of the molecule. The adsorption enthalpy ΔH_{ads} was then calculated as

$$\Delta H_{\text{ads}} = \Delta U - RT \quad (3)$$

where R is the gas constant and T is the temperature (323 K). Here, the RT term accounts for the pressure–volume term of the enthalpy, i.e., for the change from the gas phase to the condensed phase for the adsorbed molecule.

CG Simulations: Interaction of Periodic Model of Graphene with Water. To test the periodic model of graphene, we performed simulations of a CG model of a periodic graphene sheet ($12 \times 12 \text{ nm}^2$) in water. Given that Martini 3 introduces three water models to mitigate unphysical water freezing near ordered interfaces,⁸⁴ we used a mixture comprising 90% regular water beads (W) and 10% tiny water beads (TW). To ensure proper pressure convergence, we applied an anisotropic Parrinello–Rahman⁷³ barostat with a time constant of 10 ps, diagonal compressibilities of 3×10^{-4} bar⁻¹, off-diagonal compressibilities set to 0, and the reference pressure set to 1 bar using a reduced `nstpcouple` value of 10. Additional details are provided in Supporting Information S7.

Similarly, we also conducted simulations of a CG model of periodic graphene sheet ($12 \text{ nm} \times 12 \text{ nm}$) in different mixtures of water models; comprising 100% regular water beads (W), 90% regular water beads (W) and 10% small water beads (SW), 95% regular water beads (W) and 5% small water beads (SW), and 95% regular water beads (W) and 5% tiny water beads (TW). Further details are also provided in Supporting Information S7.

■ ASSOCIATED CONTENT

Data Availability Statement

Data associated with this work is publicly accessible through Zenodo at [10.5281/zenodo.14625948](https://zenodo.14625948).

■ Supporting Information

The Supporting Information is available free of charge at <https://pubs.acs.org/doi/10.1021/acs.jctc.5c00923>.

Additional results on the solid-state properties of fullerene models (lattice constants and enthalpies of sublimation for different models); additional results on free energies of transfer for fullerene models that have not been selected; potentials of mean force (PMF) profiles of fullerene dimerization and permeation into a POPC membrane, for models that have not been selected; additional information on the construction of virtual sites for the graphene model, and snippet of graphene ITP file; additional stress–strain plots for a model of graphene with optimal elastic properties; and additional information on the periodic model of graphene (PDF)

■ AUTHOR INFORMATION

Corresponding Author

Luca Monticelli — *Molecular Microbiology and Structural Biochemistry (MMSB), UMR 5086 CNRS & Université Claude Bernard Lyon 1, Lyon 69367, France; Institut National de la Santé et de la Recherche Médicale (INSERM), Lyon 69367, France; orcid.org/0000-0002-6352-4595; Email: luca.monticelli@insERM.fr*

Authors

Roshan Shrestha — *Molecular Microbiology and Structural Biochemistry (MMSB), UMR 5086 CNRS & Université Claude Bernard Lyon 1, Lyon 69367, France*

Riccardo Alessandri — *Department of Chemical Engineering, KU Leuven, 3001 Leuven, Belgium; orcid.org/0000-0003-1948-5311*

Martin Vögele — *Department of Theoretical Biophysics, Max Planck Institute of Biophysics, 60438 Frankfurt am Main, Germany; orcid.org/0000-0002-1712-358X*

Cecile Hilpert — *Molecular Microbiology and Structural Biochemistry (MMSB), UMR 5086 CNRS & Université Claude Bernard Lyon 1, Lyon 69367, France; orcid.org/0000-0002-7825-9376*

Paulo C. T. Souza — *Laboratoire de Biologie et Modélisation de la Cellule, CNRS, UMR 5239, Inserm, U1293, Université Claude Bernard Lyon 1, Lyon 69364, France; Centre Blaise Pascal de Simulation et de Modélisation Numérique, École Normale Supérieure de Lyon, Lyon 69364, France; orcid.org/0000-0003-0660-1301*

Siewert J. Marrink — *Groningen Biomolecular Sciences and Biotechnology Institute, University of Groningen, Groningen 9747 AG, The Netherlands; orcid.org/0000-0001-8423-5277*

Complete contact information is available at:

<https://pubs.acs.org/10.1021/acs.jctc.5c00923>

Author Contributions

L.M. designed the project. R.A. built initial models and performed initial calculations on fullerene. R.S. performed most simulations and analyses on fullerene and graphene. M.V. wrote code to build carbon nanotube models, and performed simulations and analyses on carbon nanotubes. C.H. wrote the code to generate coordinates and gromacs ITP files for graphene. L.M., R.A., R.S., P.C.T.S., and S.J.M. contributed to the conceptualization of the graphene and fullerene models. R.S., M.V., and L.M. wrote the initial draft. All authors discussed the results, revised the manuscript, and approved the final version of the manuscript.

Notes

The authors declare no competing financial interest.

■ ACKNOWLEDGMENTS

This work has received funding from the European Union's HORIZON 2020 Research & Innovation Programme under grant agreement no. 952924 (SUNSHINE). Computing resources were granted by the Grand équipement national de calcul intensif (GENCI) under the allocations A0120710138, A0140710138, and A0160710138. L.M., C.H., and R.S. acknowledge CC-IN2P3 (<https://cc.in2p3.fr>) for computing resources and services. P.C.T.S. would like to thank the support of the French National Center for Scientific Research (CNRS). P.C.T.S. acknowledges the support of the Centre Blaise Pascal's IT test platform at ENS de Lyon (France) for the computer facilities. The platform operates the SIDUS solution developed by Emmanuel Quemener. L.M. acknowledges funding from the Institut National de la Santé et de la Recherche Médicale (INSERM). The authors thank Alex de Vries for insightful discussions on the graphene model.

■ REFERENCES

- (1) Malik, S.; Muhammad, K.; Waheed, Y. Nanotechnology: A Revolution in Modern Industry. *Molecules* **2023**, *28* (2), No. 661.
- (2) Ahmad, A.; Verpoort, F.; Khan, A.; Ali, S. *Nanomaterials-Based Electrochemical Sensors: Properties, Applications, and Recent Advances*; Elsevier, 2023.
- (3) Holmannova, D.; Borsky, P.; Svaldakova, T.; Borska, L.; Fiala, Z. Carbon Nanoparticles and Their Biomedical Applications. *Appl. Sci.* **2022**, *12* (15), No. 7865.
- (4) Speranza, G. Carbon Nanomaterials: Synthesis, Functionalization and Sensing Applications. *Nanomaterials* **2021**, *11* (4), No. 967.
- (5) Anu Mary Ealia, S.; Saravanakumar, M. P. A Review on the Classification, Characterisation, Synthesis of Nanoparticles and Their Application. *IOP Conf. Ser.: Mater. Sci. Eng.* **2017**, *263* (3), No. 032019.
- (6) Furxhi, I.; Costa, A.; Vázquez-Campos, S.; Fito-López, C.; Hristozov, D.; Ramos, J. A. T.; Resch, S.; Cioffi, M.; Friedrichs, S.; Rocca, C.; Valsami-Jones, E.; Lynch, I.; Araceli, S. J.; Farcal, L. Status, Implications and Challenges of European Safe and Sustainable by Design Paradigms Applicable to Nanomaterials and Advanced Materials. *RSC Sustainability* **2023**, *1* (2), 234–250.
- (7) Rossi, G.; Monticelli, L. Simulating the Interaction of Lipid Membranes with Polymer and Ligand-Coated Nanoparticles. *Adv. Phys. X* **2016**, *1* (2), 276–296.
- (8) Rossi, G.; Monticelli, L. Gold Nanoparticles in Model Biological Membranes: A Computational Perspective. *Biochim. Biophys. Acta, Biomembr.* **2016**, *1858* (10), 2380–2389.
- (9) Simonelli, F.; Bochicchio, D.; Ferrando, R.; Rossi, G. Monolayer-Protected Anionic Au Nanoparticles Walk into Lipid Membranes Step by Step. *J. Phys. Chem. Lett.* **2015**, *6* (16), 3175–3179.
- (10) Canepa, E.; Salassi, S.; de Marco, A. L.; Lambruschini, C.; Odino, D.; Bochicchio, D.; Canepa, F.; Canale, C.; Dante, S.; Brescia, R.; Stellacci, F.; Rossi, G.; Relini, A. Amphiphilic Gold Nanoparticles Perturb Phase Separation in Multidomain Lipid Membranes. *Nanoscale* **2020**, *12* (38), 19746–19759.
- (11) Lin, J.; Alexander-Katz, A. Cell Membranes Open “Doors” for Cationic Nanoparticles/Biomolecules: Insights into Uptake Kinetics. *ACS Nano* **2013**, *7* (12), 10799–10808.
- (12) Bhaskara, R. M.; Linker, S. M.; Vögele, M.; Köfinger, J.; Hummer, G. Carbon Nanotubes Mediate Fusion of Lipid Vesicles. *ACS Nano* **2017**, *11* (2), 1273–1280.
- (13) Lavagna, E.; Barnoud, J.; Rossi, G.; Monticelli, L. Size-Dependent Aggregation of Hydrophobic Nanoparticles in Lipid Membranes. *Nanoscale* **2020**, *12* (17), 9452–9461.
- (14) Baoukina, S.; Monticelli, L.; Tielemans, D. P. Interaction of Pristine and Functionalized Carbon Nanotubes with Lipid Membranes. *J. Phys. Chem. B* **2013**, *117* (40), 12113–12123.
- (15) Wong-Ekkabut, J.; Baoukina, S.; Triampo, W.; Tang, I.-M.; Tielemans, D. P.; Monticelli, L. Computer Simulation Study of Fullerene Translocation through Lipid Membranes. *Nat. Nanotechnol.* **2008**, *3* (6), 363–368.
- (16) Wallace, E. J.; Sansom, M. S. P. Blocking of Carbon Nanotube Based Nanoinjectors by Lipids: A Simulation Study. *Nano Lett.* **2008**, *8* (9), 2751–2756.
- (17) Marrink, S. J.; Risselada, H. J.; Yefimov, S.; Tielemans, D. P.; de Vries, A. H. The MARTINI Force Field: Coarse Grained Model for Biomolecular Simulations. *J. Phys. Chem. B* **2007**, *111* (27), 7812–7824.
- (18) Marrink, S. J.; Monticelli, L.; Melo, M. N.; Alessandri, R.; Tielemans, D. P.; Souza, P. C. T. Two Decades of Martini: Better Beads, Broader Scope. *Wiley Interdiscip. Rev.: Comput. Mol. Sci.* **2023**, *13* (1), No. e1620, DOI: [10.1002/wcms.1620](https://doi.org/10.1002/wcms.1620).
- (19) Barnoud, J.; Rossi, G.; Monticelli, L. Lipid Membranes as Solvents for Carbon Nanoparticles. *Phys. Rev. Lett.* **2014**, *112* (6), No. 068102.
- (20) Alessandri, R.; Grünwald, F.; Marrink, S. J. The Martini Model in Materials Science. *Adv. Mater.* **2021**, *33* (24), No. e2008635.
- (21) Monticelli, L. On Atomistic and Coarse-Grained Models for C60 Fullerene. *J. Chem. Theory Comput.* **2012**, *8* (4), 1370–1378.
- (22) Vögele, M.; Köfinger, J.; Hummer, G. Molecular Dynamics Simulations of Carbon Nanotube Porins in Lipid Bilayers. *Faraday Discuss.* **2018**, *209*, 341–358.
- (23) Vögele, M.; Hummer, G. Divergent Diffusion Coefficients in Simulations of Fluids and Lipid Membranes. *J. Phys. Chem. B* **2016**, *120* (33), 8722–8732.
- (24) Vögele, M.; Köfinger, J.; Hummer, G. Hydrodynamics of Diffusion in Lipid Membrane Simulations. *Phys. Rev. Lett.* **2018**, *120* (26), No. 268104.
- (25) Gobbo, C.; Beurroies, I.; de Ridder, D.; Eelkema, R.; Marrink, S. J.; De Feyter, S.; van Esch, J. H.; de Vries, A. H. MARTINI Model for Physisorption of Organic Molecules on Graphite. *J. Phys. Chem. C* **2013**, *117* (30), 15623–15631.
- (26) Willems, N.; Urtzbereia, A.; Verre, A. F.; Iliut, M.; Lelimousin, M.; Hirtz, M.; Vijayaraghavan, A.; Sansom, M. S. P. Biomimetic Phospholipid Membrane Organization on Graphene and Graphene Oxide Surfaces: A Molecular Dynamics Simulation Study. *ACS Nano* **2017**, *11* (2), 1613–1625.
- (27) Williams, C. D.; Lísal, M. Coarse Grained Models of Graphene and Graphene Oxide for Use in Aqueous Solution. *2D Mater.* **2020**, *7* (2), No. 025025.
- (28) Barnoud, J.; Urbini, L.; Monticelli, L. C60 Fullerene Promotes Lung Monolayer Collapse. *J. R. Soc. Interface* **2015**, *12* (104), No. 20140931.
- (29) Hsu, P.-C.; Jefferies, D.; Khalid, S. Molecular Dynamics Simulations Predict the Pathways via Which Pristine Fullerenes Penetrate Bacterial Membranes. *J. Phys. Chem. B* **2016**, *120* (43), 11170–11179.
- (30) Souza, P. C. T.; Alessandri, R.; Barnoud, J.; Thallmair, S.; Faustino, I.; Grünwald, F.; Patmanidis, I.; Abdizadeh, H.; Bruininks, B. M. H.; Wassenaar, T. A.; Kroon, P. C.; Melcr, J.; Nieto, V.; Corradi, V.; Khan, H. M.; Domański, J.; Javanainen, M.; Martinez-Seara, H.; Reuter, N.; Best, R. B.; Vattulainen, I.; Monticelli, L.; Periole, X.; Tielemans, D. P.; de Vries, A. H.; Marrink, S. J. Martini 3: A General Purpose Force Field for Coarse-Grained Molecular Dynamics. *Nat. Methods* **2021**, *18* (4), 382–388.
- (31) Heiney, P. A.; Fischer, J. E.; McGhie, A. R.; Romanow, W. J.; Denenstein, A. M.; McCauley, J. P., Jr.; Smith, A. B.; Cox, D. E. Orientational Ordering Transition in Solid C60. *Phys. Rev. Lett.* **1991**, *66* (22), 2911–2914.
- (32) Girifalco, L. A. Interaction Potential for Carbon (C60) Molecules. *J. Phys. Chem. A* **1991**, *95* (14), 5370–5371.
- (33) Girifalco, L. A. Molecular Properties of Fullerene in the Gas and Solid Phases. *J. Phys. Chem. A* **1992**, *96* (2), 858–861.
- (34) Chickos, J. S.; Acree, W. E., Jr. Enthalpies of Sublimation of Organic and Organometallic Compounds. 1910–2001. *J. Phys. Chem. Ref. Data* **2002**, *31* (2), 537–698.
- (35) Alessandri, R.; Barnoud, J.; Gertsen, A. S.; Patmanidis, I.; de Vries, A. H.; Souza, P. C. T.; Marrink, S. J. Martini 3 Coarse-grained Force Field: Small Molecules. *Adv. Theory Simul.* **2022**, *5* (1), No. 2100391.
- (36) Rossi, G.; Barnoud, J.; Monticelli, L. Partitioning and Solubility of C60 Fullerene in Lipid Membranes. *Phys. Scr.* **2013**, *87* (5), No. 058503, DOI: [10.1088/0031-8949/87/05/058503](https://doi.org/10.1088/0031-8949/87/05/058503).
- (37) Pycke, B. F. G.; Chao, T.-C.; Herkes, P.; Westerhoff, P.; Halden, R. U. Beyond NC60: Strategies for Identification of Transformation Products of Fullerene Oxidation in Aquatic and Biological Samples. *Anal. Bioanal. Chem.* **2012**, *404* (9), 2583–2595.
- (38) Aschberger, K.; Johnston, H. J.; Stone, V.; Aitken, R. J.; Tran, C. L.; Hankin, S. M.; Peters, S. A. K.; Christensen, F. M. Review of Fullerene Toxicity and Exposure—Appraisal of a Human Health Risk Assessment, Based on Open Literature. *Regul. Toxicol. Pharmacol.* **2010**, *58* (3), 455–473.
- (39) Malhotra, N.; Audira, G.; Castillo, A. L.; Siregar, P.; Ruallo, J. M. S.; Roldan, M. J.; Chen, J.-R.; Lee, J.-S.; Ger, T.-R.; Hsiao, C.-D. An Update Report on the Biosafety and Potential Toxicity of Fullerene-Based Nanomaterials toward Aquatic Animals. *Oxid. Med. Cell. Longevity* **2021**, *2021*, No. 7995223.

- (40) Wallace, E. J.; D'Rozario, R. S. G.; Sanchez, B. M.; Sansom, M. S. P. A Multiscale Simulation Study of Carbon Nanotube Interactions with Designed Amphiphilic Peptide Helices. *Nanoscale* **2010**, *2* (6), 967–975.
- (41) Gul, G.; Faller, R.; Ileri-Ercan, N. Coarse-Grained Modeling of Polystyrene-Modified CNTs and Their Interactions with Lipid Bilayers. *Biophys. J.* **2023**, *122* (10), 1748–1761.
- (42) Toropov, A. A.; Leszczynska, D.; Leszczynski, J. Predicting Water Solubility and Octanol Water Partition Coefficient for Carbon Nanotubes Based on the Chiral Vector. *Comput. Biol. Chem.* **2007**, *31* (2), 127–128.
- (43) Torrens, F.; Castellano, G. (Co-)Solvent Selection for Single-Wall Carbon Nanotubes: Best Solvents, Acids, Superacids and Guest-Host Inclusion Complexes. *Nanoscale* **2011**, *3* (6), 2494–2510.
- (44) Endo, M.; Strano, M. S.; Ajayan, P. M. Potential Applications of Carbon Nanotubes. In *Carbon Nanotubes: Advanced Topics in the Synthesis, Structure, Properties and Applications*; Jorio, A.; Dresselhaus, G.; Dresselhaus, M. S., Eds.; Springer: Berlin, Heidelberg, 2008; pp 13–62.
- (45) Geng, J.; Kim, K.; Zhang, J.; Escalada, A.; Tunuguntla, R.; Comolli, L. R.; Allen, F. I.; Shnyrova, A. V.; Cho, K. R.; Munoz, D.; Wang, Y. M.; Grigoropoulos, C. P.; Ajo-Franklin, C. M.; Frolov, V. A.; Noy, A. Stochastic Transport through Carbon Nanotubes in Lipid Bilayers and Live Cell Membranes. *Nature* **2014**, *514* (7524), 612–615.
- (46) Hummer, G.; Rasaiah, J. C.; Noworyta, J. P. Water Conduction through the Hydrophobic Channel of a Carbon Nanotube. *Nature* **2001**, *414* (6860), 188–190.
- (47) Vögele, M.; Köfinger, J.; Hummer, G. Nanoporous Membranes of Densely Packed Carbon Nanotubes Formed by Lipid-Mediated Self-Assembly. *ACS Appl. Bio Mater.* **2024**, *7* (2), 528–534.
- (48) Titov, A. V.; Král, P.; Pearson, R. Sandwiched Graphene-Membrane Superstructures. *ACS Nano* **2010**, *4* (1), 229–234.
- (49) Lee, C.; Wei, X.; Kysar, J. W.; Hone, J. Measurement of the Elastic Properties and Intrinsic Strength of Monolayer Graphene. *Science* **2008**, *321* (5887), 385–388.
- (50) Ruiz, L.; Xia, W.; Meng, Z.; Keten, S. A Coarse-Grained Model for the Mechanical Behavior of Multi-Layer Graphene. *Carbon* **2015**, *82*, 103–115.
- (51) Berendsen, H. J. C.; Van Gunsteren, W. F. Molecular Dynamics Simulations: Techniques and Approaches. In *Molecular Liquids: Dynamics and Interactions*; Barnes, A. J.; Orville-Thomas, W. J.; Yarwood, J., Eds.; Springer Netherlands: Dordrecht, 1984; pp 475–500.
- (52) Jiang, J.-W.; Wang, J.-S.; Li, B. Young's Modulus of Graphene: A Molecular Dynamics Study. *Phys. Rev. B: Condens. Matter Mater. Phys.* **2009**, *80* (11), No. 113405, DOI: [10.1103/PhysRevB.80.113405](https://doi.org/10.1103/PhysRevB.80.113405).
- (53) Van Der Spoel, D.; Lindahl, E.; Hess, B.; Groenhof, G.; Mark, A. E.; Berendsen, H. J. C. GROMACS: Fast, Flexible, and Free. *J. Comput. Chem.* **2005**, *26* (16), 1701–1718.
- (54) Cambiaso, S.; Tagliabue, A.; Bochicchio, D.; Tinti, A.; Figueiredo, R.; Giacomello, F. et al. *Solid–Liquid Interfaces in MARTINI 3: Modeling Approaches and the Case Study of Silica Surfaces in Water*; ChemRxiv, 2025. DOI: [10.26434/chemrxiv-2024-bkmwz-v2.xs](https://doi.org/10.26434/chemrxiv-2024-bkmwz-v2.xs)
- (55) Schedin, F.; Geim, A. K.; Morozov, S. V.; Hill, E. W.; Blake, P.; Katsnelson, M. I.; Novoselov, K. S. Detection of Individual Gas Molecules Adsorbed on Graphene. *Nat. Mater.* **2007**, *6* (9), 652–655.
- (56) Hilpert, C.; Beranger, L.; Souza, P. C. T.; Vainikka, P. A.; Nieto, V.; Marrink, S. J.; Monticelli, L.; Launay, G. Facilitating CG Simulations with MAD: The MARTINI Database Server. *J. Chem. Inf. Model.* **2023**, *63* (3), 702–710.
- (57) Lazar, P.; Karlický, F.; Jurečka, P.; Kocman, M.; Otyepková, E.; Šafářová, K.; Otyepka, M. Adsorption of Small Organic Molecules on Graphene. *J. Am. Chem. Soc.* **2013**, *135* (16), 6372–6377.
- (58) Yannoni, C. S.; Bernier, P. F.; Bethune, D. S.; Meijer, G.; Salem, J. R. NMR determination of the bond lengths in C60. *J. Am. Chem. Soc.* **1991**, *113*, 3190.
- (59) Jorgensen, W. L.; Maxwell, D. S.; Tirado-Rives, J. Development and Testing of the OPLS All-Atom Force Field on Conformational Energistics and Properties of Organic Liquids. *J. Am. Chem. Soc.* **1996**, *118* (45), 11225–11236.
- (60) Jorgensen, W. L.; Madura, J. D.; Swenson, C. J. Optimized Intermolecular Potential Functions for Liquid Hydrocarbons. *J. Am. Chem. Soc.* **1984**, *106* (22), 6638–6646.
- (61) Berger, O.; Edholm, O.; Jähnig, F. Molecular Dynamics Simulations of a Fluid Bilayer of Dipalmitoylphosphatidylcholine at Full Hydration, Constant Pressure, and Constant Temperature. *Biophys. J.* **1997**, *72* (5), 2002–2013.
- (62) Berendsen, H. J. C.; Postma, J. P. M.; van Gunsteren, W. F.; Hermans, J. In *Interaction Models for Water in Relation to Protein Hydration*, Intermolecular Forces: Proceedings of the Fourteenth Jerusalem Symposium on Quantum Chemistry and Biochemistry Held in Jerusalem, Israel, April 13–16, 1981; Pullman, B., Ed.; Springer Netherlands: Dordrecht, 1981; pp 331–342.
- (63) Darden, T.; York, L.; Pedersen, L. Particle Mesh Ewald: An N-Log(N) Method for Ewald Sums in Large Systems. *J. Chem. Phys.* **1993**, *98*, 10089–10092.
- (64) Dickson, C. J.; Madej, B. D.; Skjevik, A. A.; Betz, R. M.; Teigen, K.; Gould, I. R.; Walker, R. C. Lipid14: The Amber Lipid Force Field. *J. Chem. Theory Comput.* **2014**, *10* (2), 865–879.
- (65) Case, D. A.; Babin, V.; Berryman, J. T.; Betz, R. M.; Cai, Q.; Cerutti, D. S.; Cheatham, T. E., III; Darden, T. A.; Duke, R. E.; Gohlke, H. et al. AMBER 14; University of California: San Francisco, 2014; pp 1–826.
- (66) Wang, J.; Wolf, R. M.; Caldwell, J. W.; Kollman, P. A.; Case, D. A. Development and Testing of a General Amber Force Field. *J. Comput. Chem.* **2004**, *25* (9), 1157–1174.
- (67) Sousa da Silva, A. W.; Vranken, W. F. ACPYPE - AnteChamber PYthon Parser Interface. *BMC Res. Notes* **2012**, *5*, No. 367.
- (68) Huang, J.; MacKerell, A. D., Jr. CHARMM36 All-Atom Additive Protein Force Field: Validation Based on Comparison to NMR Data. *J. Comput. Chem.* **2013**, *34* (25), 2135–2145.
- (69) Darden, T.; York, D.; Pedersen, L. Particle Mesh Ewald: An N-log(N) Method for Ewald Sums in Large Systems. *J. Chem. Phys.* **1993**, *98*, 10089–10092.
- (70) Essmann, U.; Perera, L.; Berkowitz, M.; Darden, T.; Lee, H.-C.; Pedersen, L. A Smooth Particle Mesh Ewald Method. *J. Chem. Phys.* **1995**, *103*, 8577–8593.
- (71) Hess, B.; Bekker, H.; Berendsen, H. J. C.; Fraaije, J. G. E. M. LINCS: A Linear Constraint Solver for Molecular Simulations. *J. Comput. Chem.* **1997**, *18* (12), 1463–1472.
- (72) Bussi, G.; Donadio, D.; Parrinello, M. Canonical Sampling through Velocity Rescaling. *J. Chem. Phys.* **2007**, *126* (1), No. 014101.
- (73) Parrinello, M.; Rahman, A. Polymorphic Transitions in Single Crystals: A New Molecular Dynamics Method. *J. Appl. Phys.* **1981**, *52*, 7182–7190, DOI: [10.1063/1.328693](https://doi.org/10.1063/1.328693).
- (74) Berendsen, H. J. C. Practical Algorithms for Dynamic Simulations. *Molecular-Dynamics Simulation of Statistical–Mechanical Systems*; Elsevier Science Ltd, 1986.
- (75) Bernetti, M.; Bussi, G. Pressure Control Using Stochastic Cell Rescaling. *J. Chem. Phys.* **2020**, *153* (11), No. 114107.
- (76) Leach, A. R. *Molecular Modelling: Principles and Applications*; Pearson Education, 2001.
- (77) Shirts, M. R.; Chodera, J. Statistically Optimal Analysis of Samples from Multiple Equilibrium States. *J. Chem. Phys.* **2008**, *129* (12), No. 124105.
- (78) Torrie, G. M.; Valleau, J. P. Nonphysical Sampling Distributions in Monte Carlo Free-Energy Estimation: Umbrella Sampling. *J. Comput. Phys.* **1977**, *23* (2), 187–199.
- (79) Kumar, S.; Rosenberg, J. M.; Bouzida, D.; Swendsen, R. H.; Kollman, P. A. THE Weighted Histogram Analysis Method for Free-energy Calculations on Biomolecules. I. The Method. *J. Comput. Chem.* **1992**, *13* (8), 1011–1021.
- (80) Hub, J. S.; de Groot, B. L.; van der Spoel, D. G_wham—A Free Weighted Histogram Analysis Implementation Including Robust

Error and Autocorrelation Estimates. *J. Chem. Theory Comput.* **2010**, *6* (12), 3713–3720.

(81) Wassenaar, T. A.; Ingólfsson, H. I.; Böckmann, R. A.; Tielemans, D. P.; Marrink, S. J. Computational Lipidomics with Insane: A Versatile Tool for Generating Custom Membranes for Molecular Simulations. *J. Chem. Theory Comput.* **2015**, *11* (5), 2144–2155.

(82) Hess, B.; Kutzner, C.; van der Spoel, D.; Lindahl, E. GROMACS 4: Algorithms for Highly Efficient, Load-Balanced, and Scalable Molecular Simulation. *J. Chem. Theory Comput.* **2008**, *4* (3), 435–447.

(83) Pronk, S.; Päll, S.; Schulz, R.; Larsson, P.; Bjelkmar, P.; Apostolov, R.; Shirts, M. R.; Smith, J. C.; Kasson, P. M.; van der Spoel, D.; Hess, B.; Lindahl, E. GROMACS 4.5: A High-Throughput and Highly Parallel Open Source Molecular Simulation Toolkit. *Bioinformatics* **2013**, *29* (7), 845–854.

(84) Iannetti, L.; Cambiaso, S.; Rasera, F.; Giacomello, A.; Rossi, G.; Bochicchio, D.; Tinti, A. The Surface Tension of Martini 3 Water Mixtures. *J. Chem. Phys.* **2024**, *161* (8), No. 084707, DOI: 10.1063/5.0221199.

CAS BIOFINDER DISCOVERY PLATFORM™

ELIMINATE DATA SILOS. FIND WHAT YOU NEED, WHEN YOU NEED IT.

A single platform for relevant, high-quality biological and toxicology research

Streamline your R&D

CAS
A division of the
American Chemical Society